Accurate Localization of a Rigid Body Using Multiple Sensors and Landmarks

Shanjie Chen, *Student Member, IEEE*, and K. C. Ho, *Fellow, IEEE*

***Abstract*—This paper develops estimators for locating a rigid body using the time measurements, and the Doppler as well if it is moving, between the sensors in the rigid body and a few landmarks outside. The challenge of rigid body localization is that in addition to the position, we are also interested in obtaining the rotation parameters of the rigid body that must belong to the special orthogonal group. The proposed estimators are non-iterative and have two steps: preliminary and refinement. The preliminary step provides a coarse estimate and the refinement step improves the first step estimate to yield an accurate solution. When the rigid body is stationary, we are able to locate the body with accuracy higher than the solutions of comparable complexity found in the literature. When the rigid body is moving, we develop an estimator that contains the additional unknowns of angular and translational velocities. Simulations show that the proposed estimators, in both stationary and moving cases, can approach the Cramer-Rao Lower Bound performance under Gaussian noise over the small error region.**

***Index Terms*—Closed-form solution, divide and conquer, GTRS, moving rigid body, position and orientation, sequential estimation.**

I. Introduction

OBTAINING the orientation and position of a rigid body is an important subject for many applications in robotics, automobiles, spacecraft, underwater vehicles, gaming and many others [1]–[4]. An inertial measurement unit (IMU), such as an accelerometer or a gyroscope, can give the orientation and position of a rigid body. It may suffer from long-term performance deviation and requires accurate calibration by additional devices [5]. Using GPS for the positioning problem could be costly as it requires complicated receivers [6] and it operates in outdoor environments only.

An alternative approach is to place a few sensors in the rigid body and uses some measurements [6]–[8] with respect to a few landmarks (simply called anchors in this paper) to identify its orientation and position. Different from the traditional sensor node localization in a network using a number of anchors [9]–[14], the relative positions of the sensors are known. Consequently, the problem reduces to finding the rotation matrix and translation vector of the sensor array on the body and it is termed as rigid body localization [6]. Rigid body localization is a challenging nonlinear constrained optimization problem. The rotation matrix and translation vector are nonlinearly related to the measurements and they are strongly coupled. In addition, the rotation matrix must belong to the special orthogonal (SO) group [15], meaning that its elements must satisfy certain quadratic constraints in 2D and cubic constraints in 3D. The difficulty of solving the problem remains even if we perform certain global parameterization of the rotation matrix, such as unit quaternion.

When the rigid body is stationary, distance (time) measurements are common. A direct solution but rather complicated to implement is the Maximum Likelihood Estimator (MLE) that is obtained through an iterative geometric descent approach, where the optimization is performed in the Riemannian manifolds [7] to satisfy the SO group constraint. The estimator requires good initial guesses for convergence to the correct solution. Under the noise free assumption, [8] derived a solution by constructing a dynamic system that evolves on the special Euclidean group $SE(3)$ where local asymptotic stability can be maintained. This method requires many numerical integrations to determine the evolving state of the system and its performance under noisy measurements is not guaranteed.

Reference [6] addresses the nonlinear estimation problem using the range-based localization technique. It converts the measurement equation to a linear form by taking the squares and eliminating the quadratic unknown terms. Two main solutions were developed, one is the constrained least squares (CLS) which is iterative and the other is the simplified constrained least squares (SCLS) that is non-iterative. They are not asymptotically efficient in general.

One may consider using CLS or SCLS to initialize an iterative implementation of the MLE to reach a better solution. The MLE is rather difficult to realize [7] since the SO group constraint must be imposed in each iteration.

Most rigid bodies of interests are often not standstill, obvious examples are UAVs and robots. Indeed, many engineering applications [5], [16]–[18] are related to the localization and tracking of a moving object. A moving rigid body has the additional parameters of angular and translational velocities. If they are known, [19] has proposed a tracking solution. They are, however, often not known without using IMU and we have not come across any solution from the literature. The need to develop a localization method for a moving rigid body with unknown velocities is evident.

In this paper, we propose closed-form solutions to the rigid body localization problem where the rigid body can be stationary or moving. The aim is to achieve better performance than the previous computationally attractive methods such as

Manuscript received December 20, 2014; revised May 16, 2015 and July 11, 2015; accepted July 21, 2015. Date of publication August 05, 2015; date of current version November 10, 2015. The associate editor coordinating the review of this manuscript and approving it for publication was Prof. Joseph Tabrikian.

The authors are with the Electrical and Computer Engineering Department, University of Missouri, Columbia, MO 65211 USA (e-mail: sjchen1984@gmail.com; hod@missouri.edu).

Color versions of one or more figures in this article are available online at http://ieeexplore.ieee.org.

Digital Object Identifier 10.1109/TSP.2015.2465356

SCLS and CLS while maintaining similar complexity. The proposed solutions use a two-step approach. The first step obtains a preliminary solution by using the divide and conquer (DAC) technique [20] that solves the individual sensor positions first and then the rotation and translation parameters with the rotation matrix structure imposed. The preliminary solution is reasonably accurate as supported by the theory of the DAC approach, but not able to reach the optimum performance due to some simplifications taken in arriving at a closed-form solution. The second step reformulates the estimation problem in terms of the correction to the preliminary solution for obtaining a better result.

In the special case of 2D scenario, we can take the advantage of the simpler rotation matrix structure so that both processing steps can be reformulated as two separate generalized trust region subproblem (GTRS) [21]–[24] optimizations in which computationally efficient closed-form solutions exist.

Finally, we proceed to solve the localization of a moving rigid body that includes the additional unknowns of angular and translational velocities. In addition to distance, we also make use of the Doppler measurements.

The approach we take to obtain the preliminary solution in step-1 is different from those in [6]. In particular, [6] solves the rotation matrix and translation vector directly from the measurements with the rotation matrix constraint imposed. It relaxes the measurement equations and removes the quadratic unknown terms, leading to a suboptimum solution. We apply the DAC approach [20] by estimating the sensor positions from the measurements first and then deducing the unknowns through the singular value decomposition (SVD). Although [6] has considered using the estimated sensor positions to solve for the translation vector, the results are not satisfactory and are worse than that from SCLS [6]. The proposed step-1 solution is able to provide better accuracy than the non-iterative SCLS solution. It has lower complexity than the iterative CLS solution [6] and does not require initialization.

The second step that we develop here is novel. We show that the second step reduces to solving a multiplicative correction matrix. Through the Euler angles formulation, the correction matrix can be obtained through the weighted least squares (WLS) minimization. If the localization is in 2D, the second step reduces to solving a GTRS optimization.

Lastly, we would like to emphasize the proposed solution of moving rigid body localization does not require the angular or translational velocities to be known. This is in contrast to [19] where the velocities are needed.

This paper is organized as follows. Section II provides the scenario for the rigid body localization problem. Section III describes the proposed method for locating a stationary rigid body. Section IV presents an additional solution for the localization problem in the 2D space. Section V focuses on moving rigid body localization. Section VI elaborates on the expected performance of the proposed methods and examines the computational complexity. Section VII supports the performance of the proposed solutions by simulations. Section VIII concludes the paper.

We shall use bold lower-case and upper-case letters to denote column vector and matrix. $\mathbf{I}$ and $\mathbf{O}$ are identity and zero matrices of appropriate size, and $\mathbf{1}$ and $\mathbf{0}$ are unity and zero vectors. $\mathbf{a}^o$ is the true value of the noisy quantity $\mathbf{a}$. $\mathrm{vec}(\mathbf{A})$ is a column vector by stacking the columns of $\mathbf{A}$, $\det(\mathbf{A})$ is the determinant, and $\mathrm{diag}(\mathbf{a})$ is a diagonal matrix formed by the elements of $\mathbf{a}$. The symbol $\odot$ represents the Hadamard product and $\otimes$ the Kronecker product. We have the matrix vectorization formula that [25]

$$\mathrm{vec}(\mathbf{XYZ}) = (\mathbf{Z}^T \otimes \mathbf{X})\mathrm{vec}(\mathbf{Y})\,. \tag{1}$$

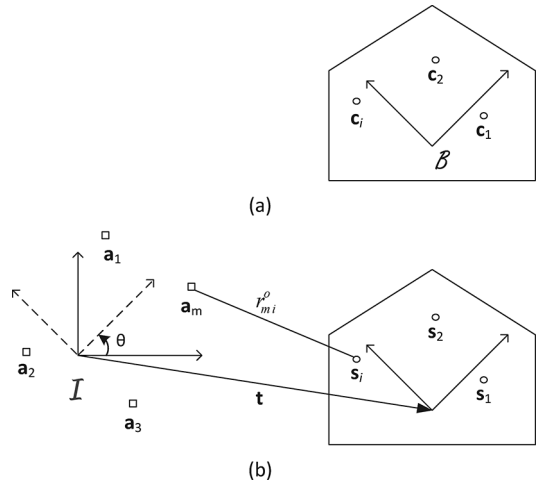

Fig. 1. An illustration for rigid body localization, shown in 2D for ease of illustration. (a) The known sensor position $\mathbf{c}_i$ in the local reference frame $\mathcal{B}$; (b) The unknown sensor position $\mathbf{s}_i$ in the inertial reference frame $\mathcal{I}$ that is related to $\mathbf{c}_i$ by (2) through the rotation and translation between the two reference frames.

II. Scenario

Fig. 1 illustrates the localization scenario. The rigid body we would like to locate has N sensors mounted whose positions at the local reference frame $\mathcal{B}$ are $\mathbf{c}_i \in \mathbb{R}^K$, where $i = 1, 2, \ldots, N$ and K is the dimension of localization. The reference frame here refers to a set of oriented orthonormal vectors at a certain position. $\mathcal{B}$ has the orientation represented by the rotation matrix $\mathbf{Q} \in \mathbb{R}^{K\times K}$ and the origin denoted by the position vector $\mathbf{t} \in \mathbb{R}^K$ with respect to the inertial reference frame $\mathcal{I}$. The rotation matrix must belong to the special orthogonal group $SO(K) = \{\mathbf{Q} \in \mathbb{R}^{K\times K} : \mathbf{Q}^T\mathbf{Q} = \mathbf{I}, \det(\mathbf{Q}) = 1\}$ [15].[1]

In $\mathcal{I}$ the position of the i-th sensor is [6]

$$\mathbf{s}_i = \mathbf{Q}\mathbf{c}_i + \mathbf{t}. \tag{2}$$

We shall determine $\mathbf{Q}$ and $\mathbf{t}$ using M anchors whose positions are exactly known at $\mathbf{a}_m \in \mathbb{R}^K$ in $\mathcal{I}$, $m = 1, 2, \ldots, M$. The anchors provide the distance measurements to the sensors which are modelled as [6]

$$r_{mi} = r^o_{mi} + v_{mi} \tag{3a}$$
$$= \|\mathbf{a}_m - \mathbf{s}_i\| + v_{mi} \tag{3b}$$
$$= \|\mathbf{a}_m - \mathbf{Q}\mathbf{c}_i - \mathbf{t}\| + v_{mi} \tag{3c}$$

[1]Note that the condition $\mathbf{Q}^T\mathbf{Q} = \mathbf{I}$ alone is not sufficient since $\det(\mathbf{Q})$ can be $+1$ or -1, and the case of $\det(\mathbf{Q}) = -1$ yields a reflection matrix that is not able to describe the rigid transformation.

where $r^o_{mi} = \|\mathbf{a}_m - \mathbf{s}_i\|$ and v_{mi} is the additive noise. The collection of all measurements together forms the vector $\mathbf{r} = \mathbf{r}^o + \mathbf{v}$. The noise vector $\mathbf{v}$ follows a zero mean Gaussian distribution with covariance matrix $\mathbf{R}_\mathbf{v}$.

For a moving rigid body, the velocity of the individual sensor in the inertial frame is $\dot{\mathbf{s}}_i$, while the motion of the entire rigid body is characterized by the angular velocity $\boldsymbol{\omega}$ and translational velocity $\dot{\mathbf{t}}$. Applying the time derivative of $\mathbf{s}_i$ in (2) gives the relation

$$\dot{\mathbf{s}}_i = [\boldsymbol{\omega}]^\times \mathbf{Q}\mathbf{c}_i + \dot{\mathbf{t}}. \tag{4}$$

$[*]^\times$ is the cross product operator matrix [15] that maps the vector $\boldsymbol{\omega}$ to a skew-symmetric matrix.[2]

The Doppler measurements from the motion of a rigid body are [26]

$$\dot{r}_{mi} = \frac{(\mathbf{s}_i - \mathbf{a}_m)^T}{r^o_{mi}}\dot{\mathbf{s}}_i + \dot{v}_{mi}. \tag{5}$$

We use the terms Doppler shift and range rate interchangeably because they differ only by a scaling factor of the propagation speed divided by the carrier frequency. The Doppler measurement vector is $\dot{\mathbf{r}} = \dot{\mathbf{r}}^o + \dot{\mathbf{v}}$ and the Doppler noise vector $\dot{\mathbf{v}}$ is zero mean Gaussian with covariance $\mathbf{R}_{\dot{\mathbf{v}}}$. Together with the distance measurement noise, $[\mathbf{v}^T, \dot{\mathbf{v}}^T]^T$ follows a zero mean Gaussian distribution with covariance matrix $\mathbf{R}$.

The problem can be stated as follows. Given the distance measurements r_{mi} and the relative sensor positions in the local frame $\mathcal{B}$, obtain the rotation matrix $\mathbf{Q}$ and the position vector $\mathbf{t}$ of the rigid body as observed in the inertial reference frame $\mathcal{I}$. If the rigid body is moving, estimate the angular and translational velocities as well through the additional Doppler measurements.

III. Stationary Rigid Body Localization

The positioning solution for stationary rigid body developed in this section is general and is applicable to both 2D and 3D cases.

A. Step-1: Preliminary Solution

Rather than obtaining $\mathbf{Q}$ and $\mathbf{t}$ directly from the measurements, we resort to the DAC approach proposed by Abel [20]. The idea is to use the sensor positions in $\mathcal{I}$ as the intermediate variables to obtain the rotation and translation parameters. Essentially, we first separate the distance measurements to N non-overlapping sets, each containing the measurements from the anchors to the same sensor. The sensor positions are solved independently from each measurement set. Next, we impose the model (2) between $\mathbf{s}_i$ and $\mathbf{c}_i$ to determine the rotation matrix and translation vector.

The estimation of a sensor position using distance measurements from a number of anchors is a well known TOA localization problem and the amount of solutions available in the literature is abundant, such as the closed-form two-stage method [27], [28] and the GTRS solution [24], [29]. The two-stage method has a lower noise threshold than the GTRS method but it is much more computationally efficient. Solving the sensor positions individually requires at least $K+1$ distance measurements for each sensor to ensure a unique solution. We shall denote the estimated sensor positions as $\hat{\mathbf{s}}_i$.

Determining the rotation and translation relationship between two sets of data points at different coordinates, $\hat{\mathbf{s}}_i$ and $\mathbf{c}_i$ in our case, is a typical problem in pattern analysis [30], [31] or general Procrustes analysis. It can be formulated as a least squares minimization problem as

$$\begin{aligned} &\min_{\mathbf{Q},\mathbf{t}} \Sigma_{i=1}^N [\hat{\mathbf{s}}_i - (\mathbf{Q}\mathbf{c}_i + \mathbf{t})]^T \mathbf{W}_i [\hat{\mathbf{s}}_i - (\mathbf{Q}\mathbf{c}_i + \mathbf{t})] \\ &\text{s.t. } \mathbf{Q} \in SO(K) \end{aligned} \tag{6}$$

where the optimal weighting $\mathbf{W}_i$ is the inverse of the covariance of $\hat{\mathbf{s}}_i$. This optimization in general does not admit a closed-form solution except for the 2D case. Alternatively, we consider the non-negative scalar weighting

$$\begin{aligned} &\min_{\mathbf{Q},\mathbf{t}} J = \Sigma_{i=1}^N w_i \|\hat{\mathbf{s}}_i - (\mathbf{Q}\mathbf{c}_i + \mathbf{t})\|^2 \\ &\text{s.t. } \mathbf{Q} \in SO(K) \end{aligned} \tag{7}$$

which corresponds to the weighting matrix of the form $\mathbf{W}_i = w_i\mathbf{I}$.

Let us denote the weighted average values

$$\bar{\mathbf{s}} = \sum_{i=1}^N w_i \hat{\mathbf{s}}_i / \sum_{i=1}^N w_i, \quad \bar{\mathbf{c}} = \sum_{i=1}^N w_i \mathbf{c}_i / \sum_{i=1}^N w_i.$$

By setting to zero the derivative of J with respect to $\mathbf{t}$, we obtain the solution of $\mathbf{t}$ as

$$\mathbf{t} = \bar{\mathbf{s}} - \mathbf{Q}\bar{\mathbf{c}}. \tag{8}$$

We shall denote $\tilde{\mathbf{s}}_i = \hat{\mathbf{s}}_i - \bar{\mathbf{s}}$ and $\tilde{\mathbf{c}}_i = \mathbf{c}_i - \bar{\mathbf{c}}$. Putting (8) back to J gives

$$\begin{aligned} J &= \Sigma_{i=1}^N w_i \|\tilde{\mathbf{s}}_i - \mathbf{Q}\tilde{\mathbf{c}}_i\|^2 \\ &= -2\,\Sigma_{i=1}^N w_i \tilde{\mathbf{s}}_i^T \mathbf{Q}\tilde{\mathbf{c}}_i + \mathcal{K} \\ &= -2\,\mathrm{trace}(\mathbf{Q}\Sigma_{i=1}^N w_i \tilde{\mathbf{c}}_i \tilde{\mathbf{s}}_i^T) + \mathcal{K} \end{aligned} \tag{9}$$

where $\mathcal{K} = \sum_{i=1}^N w_i(\|\tilde{\mathbf{s}}_i\|^2 + \|\tilde{\mathbf{c}}_i\|^2)$ is a constant independent of $\mathbf{Q}$. Note that $\mathbf{Q}^T\mathbf{Q} = \mathbf{I}$ has been used. Minimizing J is equivalent to maximizing $\mathrm{trace}(\mathbf{Q}\Sigma_{i=1}^N w_i \tilde{\mathbf{c}}_i \tilde{\mathbf{s}}_i^T)$. Let the SVD of $\Sigma_{i=1}^N w_i \tilde{\mathbf{c}}_i \tilde{\mathbf{s}}_i^T$ be $\mathbf{U}\boldsymbol{\Sigma}\mathbf{V}^T$, then the optimal solution is [31]

$$\mathbf{Q} = \mathbf{V}\mathrm{diag}([\mathbf{1}^T, \det(\mathbf{V}\mathbf{U}^T)]^T)\mathbf{U}^T, \tag{10}$$

where the length of $\mathbf{1}$ is $K-1$, and the value $\det(\mathbf{V}\mathbf{U}^T)$ ensures the resulting rotation matrix fulfills $\det(\mathbf{Q}) = 1$. Putting (10) back to (8) gives the solution for the translation vector. We shall denote the solution from step-1 as $(\hat{\mathbf{Q}}, \hat{\mathbf{t}})$.

B. Step-2: Refinement

We square both sides of distance equation (3b), ignore the second order noise term and substitute (2) to obtain [6], [32]

$$\begin{aligned} r^2_{mi} &= (\|\mathbf{a}_m - \mathbf{s}_i\| + v_{mi})^2 && \text{(11a)} \\ &\approx \|\mathbf{a}_m\|^2 - 2\mathbf{a}_m^T\mathbf{s}_i + \|\mathbf{s}_i\|^2 + n_{mi} && \text{(11b)} \\ &= \|\mathbf{a}_m\|^2 - 2\mathbf{a}_m^T(\mathbf{Q}\mathbf{c}_i + \mathbf{t}) + \|\mathbf{c}_i\|^2 + 2\mathbf{t}^T\mathbf{Q}\mathbf{c}_i \\ &\quad + \|\mathbf{t}\|^2 + n_{mi} && \text{(11c)} \end{aligned}$$

[2]It is equal to (35) in 3D or (36) in 2D.

where $n_{mi} = 2r^o_{mi}v_{mi}$. The collection of n_{mi} gives the composite noise vector $\mathbf{n}$ for the squared range values, which has a covariance matrix $\mathbf{R_n} = 4\,\mathrm{diag}(\mathbf{r}^o)\mathbf{R_v}\mathrm{diag}(\mathbf{r}^o)$ that is dependent on the true ranges. For implementation purpose, we replace the true range values by the measurements. Simulations show that the performance degradation is negligible, especially when the rigid body is far from the anchors.

Obtaining $\mathbf{Q}$ and $\mathbf{t}$ directly from the squared measurements r^2_{mi} in (11c) is difficult because it contains the nonlinear terms $\mathbf{t}^T\mathbf{Q}$ and $\|\mathbf{t}\|^2$. We handle this challenge by expressing (11c) in terms of the correction to the step-1 solution $(\hat{\mathbf{Q}}, \hat{\mathbf{t}})$ and solving for the correction instead.

We can always decompose the translation vector as $\mathbf{t} = \hat{\mathbf{t}} + \Delta\mathbf{t}$. Under the assumption that the correction is not much such that $\|\Delta\mathbf{t}\|/\|\hat{\mathbf{t}}\|$ is small enough to be neglected,

$$\|\mathbf{t}\|^2 \approx \|\hat{\mathbf{t}}\|^2 + 2\hat{\mathbf{t}}^T\Delta\mathbf{t}. \tag{12}$$

In addition,

$$\mathbf{t}^T\mathbf{Q} \approx \hat{\mathbf{t}}^T\mathbf{Q} + \Delta\mathbf{t}^T\hat{\mathbf{Q}} \tag{13}$$

where $\Delta\mathbf{t}^T\mathbf{Q} \approx \Delta\mathbf{t}^T\hat{\mathbf{Q}}$ has been used, which is valid when we ignore the second order correction between $\mathbf{Q}$ and $\mathbf{t}$ to the step-1 solution.

Using linear approximations (12) and (13) in (11c) yields

$$\begin{aligned} r^2_{mi} - (\|\hat{\mathbf{t}} - \mathbf{a}_m\|^2 + \|\mathbf{c}_i\|^2) \\ = 2(\hat{\mathbf{t}} - \mathbf{a}_m)^T\mathbf{Q}\mathbf{c}_i + 2(\hat{\mathbf{Q}}\mathbf{c}_i + \hat{\mathbf{t}} - \mathbf{a}_m)^T\Delta\mathbf{t} + n_{mi}. \end{aligned} \tag{14}$$

The refinement will be based on this equation. We should emphasize that $\mathbf{Q}$ above needs to satisfy the $SO(K)$ constraint.

It is tempted to use the same additive correction to decompose $\mathbf{Q}$ as for $\mathbf{t}$. Such a decomposition is unfavorable since it is $\mathbf{Q}$ that needs to satisfy the $SO(K)$ constraint, rather than the additive correction. Here the rotation matrix $\mathbf{Q}$ is expressed in multiplicative form as

$$\mathbf{Q} = \hat{\mathbf{Q}}\mathbf{Q}_\delta, \tag{15}$$

where $\mathbf{Q}_\delta$ is the corrective rotation matrix applied to $\hat{\mathbf{Q}}$. The factorization is unique since $\mathbf{Q}_\delta$ is equal to $\hat{\mathbf{Q}}^T\mathbf{Q}$ when premultiplying (15) by $\hat{\mathbf{Q}}^T$.

$\mathbf{Q}_\delta$ is represented by the Euler angles roll ϕ, pitch θ, and yaw ψ with sequence (1, 2, 3) [15]. Note that these Euler angles are close to zero when the preliminary solution is not far from the optimum. Using the approximation that $\cos x \approx 1$ and $\sin x \approx x$ for small x, we have for the 3D scenario [15]

$$\mathbf{Q}_\delta = \begin{bmatrix} c_\theta c_\psi & c_\theta s_\psi & -s_\theta \\ s_\phi s_\theta c_\psi - c_\phi s_\psi & s_\phi s_\theta s_\psi + c_\phi c_\psi & c_\theta s_\phi \\ c_\phi s_\theta c_\psi + s_\phi s_\psi & c_\phi s_\theta s_\psi - s_\phi c_\psi & c_\theta c_\phi \end{bmatrix} \tag{16a}$$

$$\approx \begin{bmatrix} 1 & \psi & -\theta \\ -\psi & 1 & \phi \\ \theta & -\phi & 1 \end{bmatrix} \tag{16b}$$

where $c_x = \cos x$ and $s_x = \sin x$.

In terms of the Euler angle vector $\boldsymbol{\beta} = [\phi,\ \theta,\ \psi]^T$, the vectorization of (16b) is

$$\mathrm{vec}(\mathbf{Q}_\delta) = \boldsymbol{\gamma} + \mathbf{L}\boldsymbol{\beta} \tag{17}$$

where $\boldsymbol{\gamma}$ and $\mathbf{L}$ are defined in Appendix C. For the 2D scenario, $\mathbf{Q}_\delta$ is a 2×2 matrix given by (16a) after removing the middle column and the middle row. The vectorized form (17) remains valid with different definitions of $\boldsymbol{\gamma}$, $\mathbf{L}$ and $\boldsymbol{\beta}$.

Using multiplicative correction (15) and the vectorization formula, collecting refinement equation (14) for all the measurements in a column gives

$$\breve{\mathbf{d}} - \mathbf{H}_1\boldsymbol{\gamma} = \mathbf{H}_1\mathbf{L}\boldsymbol{\beta} + \mathbf{F}_2\Delta\mathbf{t} + \mathbf{n}\,, \tag{18}$$

where $\breve{\mathbf{d}}$ is a vector whose elements are the left hand side of (14). The rows of the matrix $\mathbf{H}_1$ and $\mathbf{F}_2$ are $2[\mathbf{c}_i^T \otimes ((\hat{\mathbf{t}} - \mathbf{a}_m)^T\hat{\mathbf{Q}})]$ and $2(\hat{\mathbf{Q}}\mathbf{c}_i + \hat{\mathbf{t}} - \mathbf{a}_m)^T$, respectively. Equation (18) is a linear equation in the unknowns $\boldsymbol{\beta}$ and $\Delta\mathbf{t}$, whose WLS solution is

$$\begin{bmatrix} \hat{\boldsymbol{\beta}} \\ \Delta\hat{\mathbf{t}} \end{bmatrix} = \left(\mathbf{H}^T\mathbf{R}_\mathbf{n}^{-1}\mathbf{H}\right)^{-1}\mathbf{H}^T\mathbf{R}_\mathbf{n}^{-1}(\breve{\mathbf{d}} - \mathbf{H}_1\boldsymbol{\gamma})\,, \tag{19}$$

where $\mathbf{H} = [\mathbf{H}_1\mathbf{L}\ \ \mathbf{F}_2]$ and $\mathbf{R_n}$ is defined below (11c).

After obtaining the Euler angles, we use them to construct the original $\mathbf{Q}_\delta$ as defined in (16a) without using the small angle approximation and obtain the final estimate of $\mathbf{Q}$ from (15). Since both $\hat{\mathbf{Q}}$ and the original $\mathbf{Q}_\delta$ are in $SO(K)$, the resulting solution for $\mathbf{Q}$ will satisfy the $SO(K)$ constraint. Adding $\Delta\hat{\mathbf{t}}$ to $\hat{\mathbf{t}}$ yields the refined position vector.

The refinement solution developed here assumes the preliminary solution from step-1 is not far from the optimum. Simulations validate that the accuracy of the preliminary solution is sufficient to initiate the refinement procedure for producing a final solution approaching the CRLB accuracy. If the preliminary solution is less accurate, the refinement step can be repeated one more time by updating $\hat{\mathbf{Q}}$ and $\hat{\mathbf{t}}$.

Note that the proposed step-2 refinement solution is not tied to the step-1 solution. Other initial solutions, such as the SCLS and CLS from [6] can be used instead. Nevertheless, the more accurate the initial solution, the better will be the refined solution.

IV. 2D Case

Here we discuss the special case where there is only one rotational degree of freedom for the rigid body. In such a case, the rotational axis is perpendicular to a certain plane. To facilitate the algorithm description, we consider the anchors and sensors are on the x-y plane. Otherwise, we can augment the rotation matrix as block diagonal with blocks $\mathbf{Q}$ and 1 and add the third dimension into the translation vector $\mathbf{t}$ to make the proposed method applicable.

We shall obtain the unknowns $\mathbf{Q}$ and $\mathbf{t}$ directly from the measurements without first solving the intermediate variables $\mathbf{s}_i$. One advantage of not using the intermediate variables is that the algorithm can tolerate a larger noise level before the thresholding effect, due to the nature of the nonlinear estimation problem, occurs [33]. In addition, we only need a minimum of 2 distance measurements for each sensor as will be clear later.

When we represent $\mathbf{Q} \in \mathbb{R}^{2\times 2}$ in four variables [6], there will be four constraints from $SO(2)$ on the elements: three from $\mathbf{Q}^T\mathbf{Q} = \mathbf{I}$ and one from $\det(\mathbf{Q}) = 1$. Instead, we express the rotation matrix as

$$\mathbf{Q} = \begin{bmatrix} \cos\theta & -\sin\theta \\ \sin\theta & \cos\theta \end{bmatrix} \tag{20}$$

where θ is the rotation angle of the local frame $\mathcal{B}$ with respect to the inertial frame $\mathcal{I}$ and it is counted in the counter-clockwise direction (see Fig. 1). This representation limits $\mathbf{Q}$ to be in $SO(2)$ automatically. Through such representation, the step-1 and step-2 solutions can be obtained efficiently using the GTRS optimization technique.

A. Step-1

We shall begin with the squared range equation (11b). Stacking (11b) over the available measurements for sensor i gives the vector form

$$\mathbf{d}_i = -2\mathbf{A}^T\mathbf{s}_i + \|\mathbf{s}_i\|^2\mathbf{1} + \mathbf{n}_i \tag{21}$$

where $\mathbf{d}_i$ is a vector with elements $r_{mi}^2 - \|\mathbf{a}_m\|^2$ and $\mathbf{A}$ is a matrix with columns $\mathbf{a}_m$. Let the covariance matrix of $\mathbf{n}_i$ be $\mathbf{R}_i$, which is the i-th diagonal block of $\mathbf{R_n}$ defined below (11c). We can express $\|\mathbf{s}_i\|^2$ in terms of $\mathbf{s}_i$ in a WLS manner using the weighting matrix $\mathbf{R}_i^{-1}$ as

$$\|\mathbf{s}_i\|^2 = (\mathbf{1}^T\mathbf{R}_i^{-1}\mathbf{1})^{-1}\mathbf{1}^T\mathbf{R}_i^{-1}(\mathbf{d}_i + 2\mathbf{A}^T\mathbf{s}_i). \tag{22}$$

Putting it back to (21) and substituting (2) as well give

$$\begin{aligned}\mathbf{T}_i\mathbf{d}_i &= -2\mathbf{T}_i\mathbf{A}^T\mathbf{s}_i + \mathbf{n}_i &\text{(23a)}\\ &= -2\mathbf{T}_i\mathbf{A}^T\mathbf{Q}\mathbf{c}_i - 2\mathbf{T}_i\mathbf{A}^T\mathbf{t} + \mathbf{n}_i &\text{(23b)}\end{aligned}$$

where $\mathbf{T}_i = \mathbf{I} - \mathbf{1}\mathbf{1}^T\mathbf{R}_i^{-1}/(\mathbf{1}^T\mathbf{R}_i^{-1}\mathbf{1})$. Equation (23b) is valid as long as there are at least two measurements for each sensor so that $\mathbf{T}_i$ is not zero.

Obtaining θ directly from (23b) could be complicated since it appears as nonlinear functions $\cos\theta$ and $\sin\theta$ inside $\mathbf{Q}$. Note that optimizing over θ is equivalent to optimizing over $\mathbf{y} = [\cos\theta\ \sin\theta]^T$ with the constraint $\|\mathbf{y}\|^2 = 1$. Such an indirect approach will enable us to obtain a closed-form solution.

The vectorization of $\mathbf{Q}$ can be expressed in terms of $\mathbf{y}$ as

$$\mathrm{vec}(\mathbf{Q}) = \mathbf{\Gamma}\mathbf{y} \tag{24}$$

where $\mathbf{\Gamma}$ is a 4×2 sparse matrix with the (1, 1), (2, 2) and (4, 1) elements equal to 1 and (3, 2) element -1. Using the vectorization formula (1) in the first term on the right of (23b) yields

$$\mathbf{T}_i\mathbf{d}_i = -2(\mathbf{c}_i^T \otimes \mathbf{T}_i\mathbf{A}^T)\mathbf{\Gamma}\mathbf{y} - 2\mathbf{T}_i\mathbf{A}^T\mathbf{t} + \mathbf{n}_i \tag{25}$$

which is linear in the unknowns $\mathbf{y}$ and $\mathbf{t}$. Since they are common in all of the N sensors, stacking the above equation over i forms the vector equation

$$\bar{\mathbf{d}} = \mathbf{E}_1\mathbf{y} + \mathbf{E}_2\mathbf{t} + \mathbf{n} \tag{26}$$

where $\bar{\mathbf{d}}$ is the concatenation of the subvectors $\mathbf{T}_i\mathbf{d}_i$, and $\mathbf{E}_1$ and $\mathbf{E}_2$ are matrices formed by stacking the blocks $-2(\mathbf{c}_i^T \otimes \mathbf{T}_i\mathbf{A}^T)\mathbf{\Gamma}$ and $-2\mathbf{T}_i\mathbf{A}^T$.

The translation parameter $\mathbf{t}$ is unconstrained. The WLS solution for $\mathbf{t}$ in terms of $\mathbf{y}$ is

$$\mathbf{t} = \left(\mathbf{E}_2^T\mathbf{R_n}^{-1}\mathbf{E}_2\right)^{-1}\mathbf{E}_2^T\mathbf{R_n}^{-1}(\bar{\mathbf{d}} - \mathbf{E}_1\mathbf{y}) \tag{27}$$

where the weighting matrix is $\mathbf{R_n}^{-1}$ [34]. Let $\mathbf{P} = \mathbf{I} - \mathbf{E}_2\left(\mathbf{E}_2^T\mathbf{R_n}^{-1}\mathbf{E}_2\right)^{-1}\mathbf{E}_2^T\mathbf{R_n}^{-1}$. Putting the estimated $\mathbf{t}$ (27) back to (26) yields

$$\mathbf{P}\bar{\mathbf{d}} = \mathbf{P}\mathbf{E}_1\mathbf{y} + \mathbf{n}. \tag{28}$$

We now need to solve the constrained optimization problem for $\mathbf{y}$:

$$\begin{aligned}\min_{\mathbf{y}} &(\mathbf{P}\bar{\mathbf{d}} - \mathbf{P}\mathbf{E}_1\mathbf{y})^T\mathbf{R_n}^{-1}(\mathbf{P}\bar{\mathbf{d}} - \mathbf{P}\mathbf{E}_1\mathbf{y})\\ &= (\bar{\mathbf{d}} - \mathbf{E}_1\mathbf{y})^T\mathbf{R_n}^{-1}\mathbf{P}(\bar{\mathbf{d}} - \mathbf{E}_1\mathbf{y})\\ &\text{s.t. } \|\mathbf{y}\|^2 = 1,\end{aligned} \tag{29}$$

where we have used $\mathbf{P}^T\mathbf{R_n}^{-1}\mathbf{P} = \mathbf{R_n}^{-1}\mathbf{P}$.

This quadratic optimization problem with a quadratic equality constraint can be solved by GTRS [23], [24] efficiently to obtain the global minimum solution. In particular, the solution is

$$\mathbf{y}(\lambda) = (\mathbf{E}_1^T\mathbf{R_n}^{-1}\mathbf{P}\mathbf{E}_1 + \lambda\mathbf{I}_2)^{-1}\mathbf{E}_1^T\mathbf{R_n}^{-1}\mathbf{P}\bar{\mathbf{d}} \tag{30}$$

and λ is the largest real root of

$$\begin{aligned}\varphi(\lambda) &= \|\mathbf{y}(\lambda)\|^2 - 1\\ \lambda &\in \left(-\lambda_{\min}(\mathbf{E}_1^T\mathbf{R_n}^{-1}\mathbf{P}\mathbf{E}_1), \infty\right)\end{aligned} \tag{31}$$

where $\lambda_{\min}(*)$ is the smallest eigenvalue of $(*)$. The smallest eigenvalue is straightforward to obtain since the matrix $\mathbf{E}_1^T\mathbf{R_n}^{-1}\mathbf{P}\mathbf{E}_1$ has a size of 2 only.

The numerator of $\varphi(\lambda)$ is quartic in λ and the root finding is straightforward to implement. Once we obtain the solution $\mathbf{y}$ (and hence θ), $\mathbf{t}$ is immediately available from (27).

Rather than using the above procedure of expressing $\mathbf{t}$ in terms of $\mathbf{y}$ and solving $\mathbf{y}$ through (29), an alternative is to obtain them together by considering $\boldsymbol{\xi} = [\mathbf{y}^T, \mathbf{t}^T]^T$ as a single unknown in (26) through the minimization of $(\bar{\mathbf{d}} - \mathbf{E}\boldsymbol{\xi})^T\mathbf{R_n}^{-1}(\bar{\mathbf{d}} - \mathbf{E}\boldsymbol{\xi})$ s.t. $\boldsymbol{\xi}^T\mathbf{P}\boldsymbol{\xi} = 1$ using GTRS, where $\mathbf{E} = [\mathbf{E}_1, \mathbf{E}_2]$ and $\mathbf{P} = \mathrm{diag}(\mathbf{I}_2, \mathbf{O}_2)$. Solving them together can reduce computation if M and N are large. It can be shown analytically that both procedures will give the same solution of $\mathbf{y}$ and $\mathbf{t}$.

B. Step-2

With the solution $\hat{\mathbf{Q}}$ and $\hat{\mathbf{t}}$ from step-1, applying the vectorization formula (1) and $\mathrm{vec}(\mathbf{Q})$ in (24) to the first term on the right of the refinement equation (14) gives

$$r_{mi}^2 - (\|\hat{\mathbf{t}} - \mathbf{a}_m\|^2 + \|\hat{\mathbf{t}}\|^2) \approx \mathbf{f}_{mi,1}^T\mathbf{y} + \mathbf{f}_{mi,2}^T\Delta\mathbf{t} + n_{mi} \tag{32}$$

where

$$\begin{aligned}\mathbf{f}_{mi,1}^T &= 2[\mathbf{c}_i^T \otimes (\hat{\mathbf{t}} - \mathbf{a}_m)^T]\mathbf{\Gamma}\\ \mathbf{f}_{mi,2}^T &= 2(\hat{\mathbf{Q}}\mathbf{c}_i + \hat{\mathbf{t}} - \mathbf{a}_m)^T.\end{aligned} \tag{33}$$

Collecting the equations for all distance measurements into a single column forms

$$\breve{\mathbf{d}} = \mathbf{F}_1\mathbf{y} + \mathbf{F}_2\Delta\mathbf{t} + \mathbf{n} \tag{34}$$

where $\breve{\mathbf{d}}$, $\mathbf{F}_1$ and $\mathbf{F}_2$ are the vector and matrices by collecting the elements on the left side and the rows $\mathbf{f}_{mi,1}^T$ and $\mathbf{f}_{mi,2}^T$. Equation (34) has the same structure as (26) in step-1 and the same

procedure by using GTRS applies to the refinement as well to obtain the final estimates of $\mathbf{y}$ and $\Delta\mathbf{t}$. Adding the estimate $\Delta\mathbf{t}$ to $\hat{\mathbf{t}}$ yields the improved solution for $\mathbf{t}$.

V. Moving Rigid Body Localization

We have so far considered the rigid body is stationary. There are many occasions in practice that the rigid body has motion, for example, a vehicle moving on the ground or an aircraft flying in the air. Simply pretending a moving rigid body is stationary will lead to poor localization performance. Assuming the angular and translational velocities are known may not be reasonable. We shall extend the study to localize a moving rigid body by estimating $\mathbf{Q}$, $\mathbf{t}$, $\boldsymbol{\omega}$ and $\dot{\mathbf{t}}$ using both the distance and Doppler measurements.

In the sensor velocity model (4), the matrix $[\boldsymbol{\omega}]^\times$ is [15]

$$[\boldsymbol{\omega}]^\times = \begin{bmatrix} 0 & -\omega_3 & \omega_2 \\ \omega_3 & 0 & -\omega_1 \\ -\omega_2 & \omega_1 & 0 \end{bmatrix} \tag{35}$$

for the 3D case and

$$[\omega]^\times = \begin{bmatrix} 0 & -\omega \\ \omega & 0 \end{bmatrix} \tag{36}$$

for the 2D case. The vectorized form of $[\boldsymbol{\omega}]^\times$ that packs the angular velocity components in a vector is

$$\mathrm{vec}([\boldsymbol{\omega}]^\times) = \boldsymbol{\Phi}\boldsymbol{\omega} \tag{37}$$

where

$$\boldsymbol{\Phi} = \begin{bmatrix} 0 & 0 & 0 & 0 & 0 & 1 & 0 & -1 & 0 \\ 0 & 0 & -1 & 0 & 0 & 0 & 1 & 0 & 0 \\ 0 & 1 & 0 & -1 & 0 & 0 & 0 & 0 & 0 \end{bmatrix}^T, \quad \boldsymbol{\omega} = [\omega_1, \omega_2, \omega_3]^T \tag{38}$$

in the 3D case and

$$\boldsymbol{\Phi} = [0, 1, -1, 0]^T, \quad \boldsymbol{\omega} = \omega \tag{39}$$

in the 2D case.

Rather than using Doppler equation (5) directly, we multiply it and the distance equation (3a) to obtain

$$r_{mi}\dot{r}_{mi} = \mathbf{s}_i^T\dot{\mathbf{s}}_i - \mathbf{a}_m^T\dot{\mathbf{s}}_i + \dot{r}_{mi}v_{mi} + r_{mi}\dot{v}_{mi} \tag{40}$$

where the second order noise term $v_{mi}\dot{v}_{mi}$ is neglected.

It is straightforward to verify $\mathbf{c}_i^T\mathbf{Q}^T[\boldsymbol{\omega}]^\times\mathbf{Q}\mathbf{c}_i = 0$ since $[\boldsymbol{\omega}]^\times$ is skew-symmetric. Substituting $\mathbf{s}_i$ in (2) and $\dot{\mathbf{s}}_i$ in (4) relates (40) to the unknowns to be found:

$$r_{mi}\dot{r}_{mi} = (\mathbf{t} - \mathbf{a}_m)^T[\boldsymbol{\omega}]^\times\mathbf{Q}\mathbf{c}_i + (\mathbf{Q}\mathbf{c}_i + \mathbf{t} - \mathbf{a}_m)^T\dot{\mathbf{t}} + \dot{r}_{mi}v_{mi} + r_{mi}\dot{v}_{mi}. \tag{41}$$

The unknowns appear coupled with each other. The first term on the right contains the products of three unknowns and the second two. We shall follow the two-step approach to obtain a solution, where the first step provides a coarse preliminary solution and the second uses the preliminary solution to yield the final solution.

A. Step-1

Using the processing described in Sections III or IV, we are able to obtain an estimate of the rotation matrix and translation vector, which is denoted as $(\hat{\mathbf{Q}}, \hat{\mathbf{t}})$. Approximating $\mathbf{Q}$ and $\mathbf{t}$ by the estimates $(\hat{\mathbf{Q}}, \hat{\mathbf{t}})$ gives a linear equation in $\boldsymbol{\omega}$ and $\dot{\mathbf{t}}$ from (41),

$$r_{mi}\dot{r}_{mi} = [(\hat{\mathbf{Q}}\mathbf{c}_i)^T \otimes (\hat{\mathbf{t}} - \mathbf{a}_m)^T]\boldsymbol{\Phi}\boldsymbol{\omega} + (\hat{\mathbf{Q}}\mathbf{c}_i + \hat{\mathbf{t}} - \mathbf{a}_m)^T\dot{\mathbf{t}} + \dot{r}_{mi}v_{mi} + r_{mi}\dot{v}_{mi}, \tag{42}$$

where $[\boldsymbol{\omega}]^\times$ is expressed in the vectorized form (37) after applying the vectorization formula. Equation (42) is linear in $\boldsymbol{\omega}$ and $\dot{\mathbf{t}}$. Applying the WLS minimization over the available measurements yields their estimates $\hat{\boldsymbol{\omega}}$ and $\hat{\dot{\mathbf{t}}}$, where the weighting matrix is [34]

$$\left([\mathrm{diag}(\dot{\mathbf{r}})^T, \mathrm{diag}(\mathbf{r})^T]^T\mathbf{R}[\mathrm{diag}(\dot{\mathbf{r}}), \mathrm{diag}(\mathbf{r})]\right)^{-1}. \tag{43}$$

Using both the distance and Doppler measurements will give more accurate sensor position estimates than using distances only as in Section III-A and hence better $(\hat{\mathbf{Q}}, \hat{\mathbf{t}})$. The closed-form estimator from [26] that was developed for joint position and velocity estimation using TDOAs and FDOAs can be modified for this purpose. We summarize the major steps in Appendix D. The readers are referred to [26] for additional details.

B. Step-2

The solution from step-1, $(\hat{\mathbf{Q}}, \hat{\mathbf{t}}, \hat{\boldsymbol{\omega}}, \hat{\dot{\mathbf{t}}})$, will not reach the optimum performance since we do not consider $\mathbf{Q}$ and $\mathbf{t}$ as unknowns when solving $\boldsymbol{\omega}$ and $\dot{\mathbf{t}}$. We shall determine the amount of correction for the step-1 preliminary estimate to obtain the final solution.

Putting (15), $\mathbf{t} = \hat{\mathbf{t}} + \Delta\mathbf{t}$, $\boldsymbol{\omega} = \hat{\boldsymbol{\omega}} + \Delta\boldsymbol{\omega}$, and $\dot{\mathbf{t}} = \hat{\dot{\mathbf{t}}} + \Delta\dot{\mathbf{t}}$, (41) becomes

$$\begin{aligned} &r_{mi}\dot{r}_{mi} - \hat{\mathbf{t}}^T\hat{\dot{\mathbf{t}}} + \mathbf{a}_m^T\hat{\dot{\mathbf{t}}} \\ &= (\hat{\mathbf{t}}^T[\hat{\boldsymbol{\omega}}]^\times - \mathbf{a}_m^T[\hat{\boldsymbol{\omega}}]^\times + \hat{\dot{\mathbf{t}}}^T)\hat{\mathbf{Q}}\mathbf{Q}_\delta\mathbf{c}_i + ([\hat{\boldsymbol{\omega}}]^\times\hat{\mathbf{Q}}\mathbf{c}_i + \hat{\dot{\mathbf{t}}})^T\Delta\mathbf{t} \\ &\quad + [(\hat{\mathbf{Q}}\mathbf{c}_i)^T \otimes (\hat{\mathbf{t}} - \mathbf{a}_m)^T]\boldsymbol{\Phi}\Delta\boldsymbol{\omega} + (\hat{\mathbf{Q}}\mathbf{c}_i + \hat{\mathbf{t}} - \mathbf{a}_m)^T\Delta\dot{\mathbf{t}} \\ &\quad + \dot{r}_{mi}v_{mi} + r_{mi}\dot{v}_{mi} \end{aligned} \tag{44}$$

where the second and third order correction terms have been ignored. Note that this corresponds to setting $\mathbf{Q}_\delta$ to identity when multiplied with the other correction terms. Using the vectorization formula (1) and $\mathrm{vec}(\mathbf{Q}_\delta)$ in (17), the first term on the right of (44) becomes

$$\begin{aligned} &(\hat{\mathbf{t}}^T[\hat{\boldsymbol{\omega}}]^\times - \mathbf{a}_m^T[\hat{\boldsymbol{\omega}}]^\times + \hat{\dot{\mathbf{t}}}^T)\hat{\mathbf{Q}}\mathbf{Q}_\delta\mathbf{c}_i \\ &\quad = [\mathbf{c}_i^T \otimes (\hat{\mathbf{t}}^T[\hat{\boldsymbol{\omega}}]^\times - \mathbf{a}_m^T[\hat{\boldsymbol{\omega}}]^\times + \hat{\dot{\mathbf{t}}}^T)\hat{\mathbf{Q}}](\boldsymbol{\gamma} + \mathbf{L}\boldsymbol{\beta}). \end{aligned} \tag{45}$$

Now (44) is linear in the amount of corrections $\boldsymbol{\beta}$, $\Delta\mathbf{t}$, $\Delta\boldsymbol{\omega}$ and $\Delta\dot{\mathbf{t}}$.

Equation (18) provides the distance equations in terms of the amounts of corrections for $\mathbf{Q}$ and $\mathbf{t}$. To make use of both distance and Doppler measurements, we stack (18) and (44) to-

gether to form a matrix equation. Applying the WLS minimization with the weighting [34]

$$(\mathbf{KRK}^T)^{-1},\ \mathbf{K} = \begin{bmatrix} 2\mathrm{diag}(\mathbf{r}) & \mathbf{O} \\ \mathrm{diag}(\dot{\mathbf{r}}) & \mathrm{diag}(\mathbf{r}) \end{bmatrix} \tag{46}$$

yields the solution of the correction terms. Adding them to the step-1 preliminary solution gives the final estimate of the unknowns.

In the specific case of 2D, we can use the vectorized representation (24) instead and the first term on the right of (44) is expressed as

$$(\hat{\mathbf{t}}^T[\hat{\omega}]^\times - \mathbf{a}_m^T[\hat{\omega}]^\times + \hat{\dot{\mathbf{t}}}^T)\mathbf{Q}\mathbf{c}_i = [\mathbf{c}_i^T \otimes (\hat{\mathbf{t}}^T[\hat{\omega}]^\times - \mathbf{a}_m^T[\hat{\omega}]^\times + \hat{\dot{\mathbf{t}}}^T)]\mathbf{\Gamma}\mathbf{y}. \tag{47}$$

Applying GTRS with the constraint $\|\mathbf{y}\|^2 = 1$ will solve the WLS optimization problem from the distance refinement equation (34) and the Doppler refinement equation (44) for θ and the corrections.

VI. Performance

A. Accuracy

The estimation performance is limited by the CRLB over the small error region where the estimation bias is negligible compared to the variance. Strictly speaking the CRLB is for an unbiased estimator only. Localization is a nonlinear estimation problem that often leads to a biased estimator. However, the CRLB has been used extensively in the literature as a reference for the localization performance, due to its simplicity of computation and good prediction on the performance limit over the small error region [34]. Under the distance measurement model (3a) and the $SO(K)$ constraint on $\mathbf{Q}$, the CRLBs for $\mathbf{Q}$ and $\mathbf{t}$ of a stationary rigid body have been evaluated in [6]. The CRLBs for θ and $\mathbf{t}$ in the 2D case is provided in Appendix A. For a moving rigid body, the CRLBs for the unknown parameters are derived in Appendix B. In the simulation study of Section VII, we shall use the CRLB as a reference for performance evaluations of the proposed solutions. To supplement and support the simulations presented in the next Section, we illustrate below some rationale and insight about the performance of the proposed methods.

Let us begin with the stationary rigid body localization algorithm in Section III. The first step uses DAC to obtain a preliminary solution and the second estimates the correction to the step-1 solution. The DAC approach solves first the sensor positions and then the rotation and translation variables. Without considering the position relationship (2) among different sensors, many localization algorithms from the literature [28], [35], [36] can provide sensor position estimates that attain the CRLB accuracy. It can be shown directly through the theory of DAC [20] that when the measurements corresponding to different sensors are independent, setting the weighting factor $\mathbf{W}_i$ in optimization (6) to the Fisher information matrix (inverse of the CRLB matrix) for $\mathbf{s}_i$ will yield a solution of the rotation and translation parameters reaching the CRLB. Unfortunately such a setting does not lead to a simple closed-form solution (except for the 2D case). We therefore set $\mathbf{W}_i$ to a scalar weighting. Such setting results in suboptimum performance but enables a simple and reasonably accurate solution. This is in contrast to the approach in [6] by eliminating the $\|\mathbf{s}_i\|^2$ terms of (11b), which seems to be more significant in contributing to the loss in accuracy.

In the step-2 refinement, we reformulate the squared range equation (11c) in terms of the corrections to the unknowns with respect to the step-1 solution. It has been demonstrated [32] that with inverse range weighting, the squared range equation approximates the original range equation when the measurement noise is small. The resulting refinement equation (18) embeds the $SO(K)$ constraint through the multiplicative correction representation (15). It follows a linear model and the corresponding WLS solution (19), which is the same as the minimum variance unbiased (MVU) estimator, can reach the CRLB accuracy [34]. Consequently, we would expect the step-2 solution would be able to approach the CRLB performance over the small error region, provided that the amounts of correction relative to the actual values are not large so that (18) is reasonably accurate although ignoring the second order correction terms.

We next turn to the solution for the specific case of 2D presented in Section IV. This solution remains to use the two-step approach but the solution in each step uses the GTRS optimization. The solution here is expected to tolerate larger amount of noise before the thresholding effect occurs since the step-1 solution is obtained directly from the measurement equations without using the intermediate variables $\mathbf{s}_i$. Another interesting property is that it solves the rotation matrix directly in step-2 and does not require the correction angle formulation for the rotation matrix. As a result, the step-2 processing can accommodate larger amount of rotation correction.

For the moving rigid body localization elaborated in Section V, the solution framework is similar to what we did before in using two steps. The Doppler measurement from (5) is exploited using the transformed equation (40). Previous studies [26] showed that such a transformed equation provides nearly the same information as the original under small noise condition. The transformed equation is used in estimating the initial estimates of the angular and translational velocities in step-1 and their correction amounts in step-2. The refinement equations (18) and (44) for step-2 both follow linear models with respect to the correction terms. The resulting WLS solution (equivalent to the MVU estimator) will provide the CRLB accuracy [34] under the models. Consequently, it is expected the performance of the final solution will not deviate too much from the CRLB over the small error region when the amount of corrections relative to the true values are not significant so that the second and higher order correction terms can be neglected in (18) and (44).

B. Computational Complexity

We shall examine the computational complexity of the proposed methods for the stationary rigid body case and compare it with SCLS and CLS. The complexity is shown in big O expressions in terms of the number of anchors M, the number of sensors N and the localization dimension K (2 or 3), with the diagonal structure of $\mathbf{R_n}$ exploited. Note that the expressions

illustrate the asymptotic complexity that is valid when M and N are sufficiently large.

For the proposed method in Section III, step-1 requires $O(K^2MN)$ flops to estimate the sensor positions and $O(K^3)$ flops for an SVD to obtain the preliminary solution. Step-2 takes $O(MN)$ flops to form the refinement equations and apply the WLS processing to generate the final solution.

For the algorithm of 2D localization in Section IV, in each step, forming the equations for optimization or GTRS computation when jointly estimating $\mathbf{y}$ and $\mathbf{t}$ takes about $O(MN)$ flops.

For reference purpose, we estimate that the complexity of SCLS is $O(MN\max(M,N))$ flops + $O(K^3)$ flops, where $O(K^3)$ is for SVD. It is $O(M^3N^3)$ flops + $O(K^2MN)L$ flops for CLS, where L is the number of iterations. It is clear when M and N are sufficiently large, the proposed algorithms have lower complexity. If M and N are not large, the proposed algorithms have similar complexity with SCLS and CLS, as illustrated in the simulations.

VII. Simulations

We shall evaluate the performance of the proposed solutions for localization in 3D and 2D, using a number of geometries with randomly generated anchor positions. The CRLB is served here as a performance reference. We also include the results using the closed-form SCLS and the iterative CLS solution from [6] for comparison (please refer to Appendix E for some details of our implementations of SCLS and CLS).

There are $M = 6$ anchors and they are placed at uniformly distributed i.i.d. coordinates in a cube (3D case) or a square (2D case) having a length of 100 units centered at the origin in the inertial reference frame $\mathcal{I}$. To avoid degenerate geometry that yields poor performance, the separation between two anchors is at least 15 units. We generate $G = 200$ realizations of anchor configurations and the results reported are the averages over them. The number of ensemble runs is $L = 1000$ for a given anchor geometry. Each sensor is able to acquire the measurements from all anchors. The rigid body settings and sensor configurations will be specified later. The true distance and range rate values in the weighting matrices of the proposed algorithms are replaced by the noisy measurements throughout the simulations.

The root mean squared error (RMSE) of a parameter estimate $(*)$ is computed using

$$\mathrm{RMSE}(*) = \sqrt{\frac{1}{LG}\sum_{g=1}^{G}\sum_{l=1}^{L}\|(\hat{*})^{(g,l)} - (*)\|^2} \qquad (48)$$

where $(\hat{*})^{(g,l)}$ is the estimation for $(*)$ at the l-th ensemble run for the g-th anchor configuration. The norm is Euclidean when $(*)$ is a vector and Frobenius when $(*)$ is a matrix. Similarly, the estimation bias of $(*)$ is calculated by

$$\mathrm{bias}(*) = \sqrt{\frac{1}{G}\sum_{g=1}^{G}\left\|\frac{1}{L}\sum_{l=1}^{L}(\hat{*})^{(g,l)} - (*)\right\|^2}. \qquad (49)$$

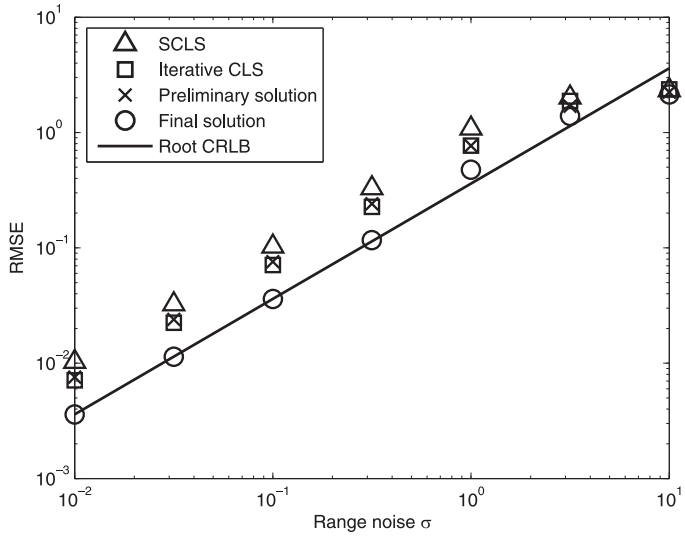

Fig. 2. Performance for rotation matrix $\mathbf{Q}$ estimation in the 3D case, averaged over 200 realizations of anchor positions.

A. Stationary Rigid Body

The distance measurement noise is uncorrelated. Often the sensor array is small and far away from the anchors. We therefore set the noise powers of distances from a given anchor to all the sensors to be the same, but different for different anchors to exercise better the algorithm performance. The noise standard deviations σ_{mi}, $m = 1, 2, \ldots, 6$, for the six anchors are $\frac{\sigma}{6}[1, 2, 3, 4, 5, 6]$.

1) 3D Case: We first evaluate the performance of the solution presented in Section III using a 3D localization scenario. The performance of the method for the 2D scenario is similar. The positions of the rigid body sensors are

$$\mathbf{C} = 3\begin{bmatrix} 0.5 & 1.5 & 1.5 & 0.5 & 1 \\ 0 & 0 & 1.5 & 1.5 & 1 \\ 0 & 0 & 0 & 0 & 1 \end{bmatrix}$$

in $\mathcal{B}$, where each column is the sensor position $\mathbf{c}_i$. It is the rectangle based pyramid used in [6]. The orientation of the rigid body is set as follows: the two reference frames coincide at the beginning, then the rigid body rotates 20 deg, -25 deg, and 10 deg with respect to x, y, z axes of $\mathcal{I}$ in sequence. The translation vector is $\mathbf{t} = [100\ 100\ 50]^T$. In the proposed method, the two-stage estimator [28] is used to obtain $\hat{\mathbf{s}}_i$ estimates in step-1 and the scalar weighting factors w_i is set to unity.

Fig. 2 shows the RMSE of the rotation matrix $\mathbf{Q}$ estimate, where the solid line is the root CRLB. The proposed step-1 preliminary solution (shown by cross-symbol), is suboptimum as expected. However, the step-2 solution (circle-symbol) is able to reach the CRLB performance when the measurement noise deviation σ is not larger than $10^{-0.5}$ (0.32). Compared to SCLS (triangle-symbol), the step-1 solution is better. Iterative CLS (rectangle-symbol) can only achieve similar performance as the proposed step-1 solution, even though it requires more computation. The proposed step-2 solution provides about 3 dB reduction in RMSE over the iterative CLS solution in the small error region.

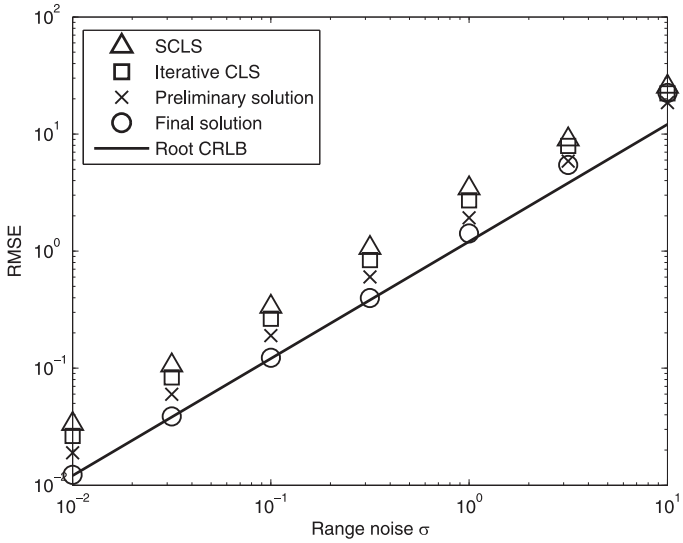

Fig. 3. Performance for position $\mathbf{t}$ estimation in the 3D case, averaged over 200 realizations of anchor positions.

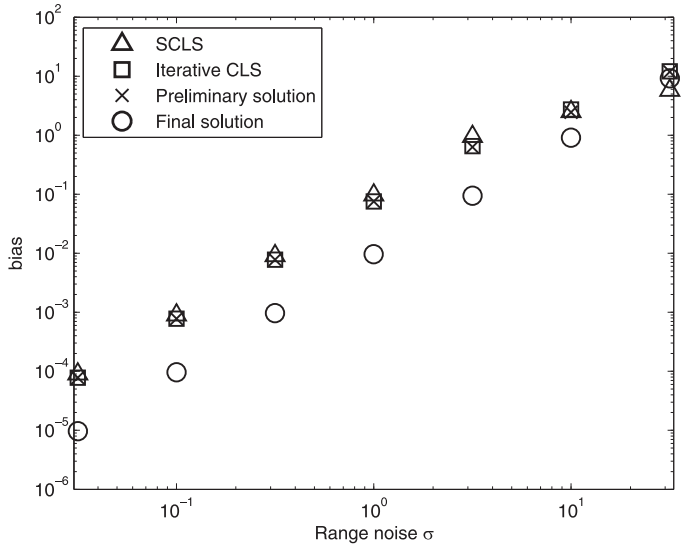

Fig. 5. Bias for position $\mathbf{t}$ estimation in the 3D case, averaged over 200 realizations of anchor positions.

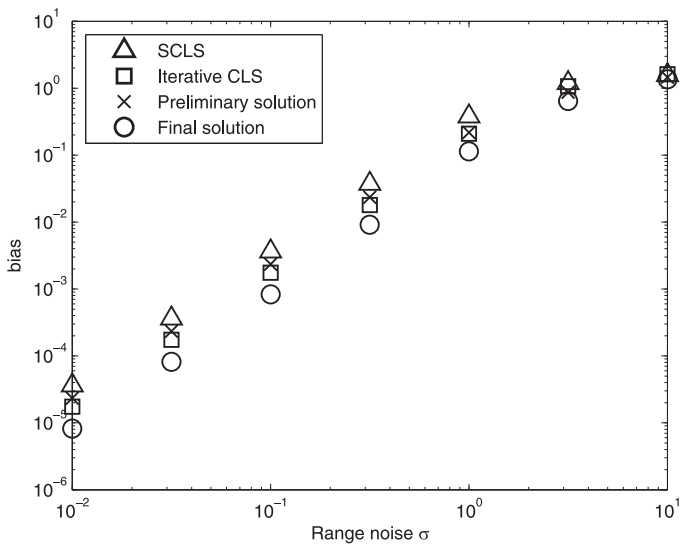

Fig. 4. Bias for rotation matrix $\mathbf{Q}$ estimation in the 3D case, averaged over 200 realizations of anchor positions.

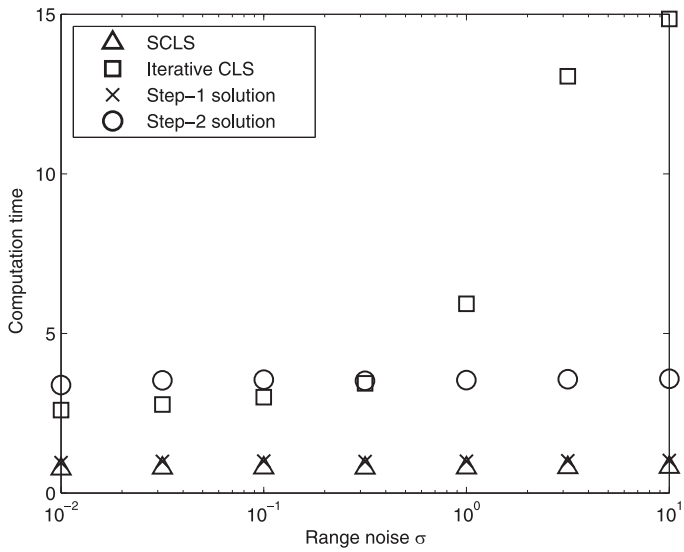

Fig. 6. Computation time (millisecond) in each Monte-Carlo run in the 3D case, averaged over 200 realizations of anchor positions.

Fig. 3 gives the RMSE performance of the translation vector $\mathbf{t}$ estimate. The observations are similar to those in Fig. 2. It is interesting to see that the step-1 solution gives better accuracy than CLS. The step-2 solution has about 3.3 dB improvement over CLS.

Figs. 4–5 are the results for estimation bias. We observe consistent behaviors in both rotation and translation that the proposed step-2 solution yields the smallest bias and the SCLS has the largest, while the proposed step-1 and the iterative CLS solution have comparable results.

Fig. 6 illustrates the computation times (millisecond) for the different solutions obtained from MATLAB implementations. The step-1 solution takes slightly larger computation than the SCLS method. The proposed step-2 solution requires the largest computation. It is the price we pay for achieving better results approaching the CRLB. The complexity of CLS rises quickly if the noise deviation σ is larger than $10^{-0.5}$ (0.32), due to larger number of iterations needed.

2) 2D Case: We next examine the proposed algorithm in Section IV, which is for the special situation where the localization is in 2D. The sensor geometry is a square given by

$$\mathbf{C} = 5\begin{bmatrix} 0 & 1 & 1 & 0 \\ 0 & 0 & 1 & 1 \end{bmatrix}$$

in the local reference frame $\mathcal{B}$. The rigid body has orientation $\theta = 20$ deg and translation $\mathbf{t} = [100\ 100]^T$ with respect to $\mathcal{I}$.

Fig. 7 gives the RMSE for the orientation θ and Fig. 8 for the translation $\mathbf{t}$. The behaviors of the different methods are similar for both parameters. The proposed step-1 solution provides 1.8 dB RMSE improvement in θ and 1.2 dB in $\mathbf{t}$ over the SCLS solution. The CLS method can only give comparable performance with the step-1 solution. The step-2 solution has 7.1 dB and 2.6 dB improvements for θ and $\mathbf{t}$ compared to the CLS solution, and

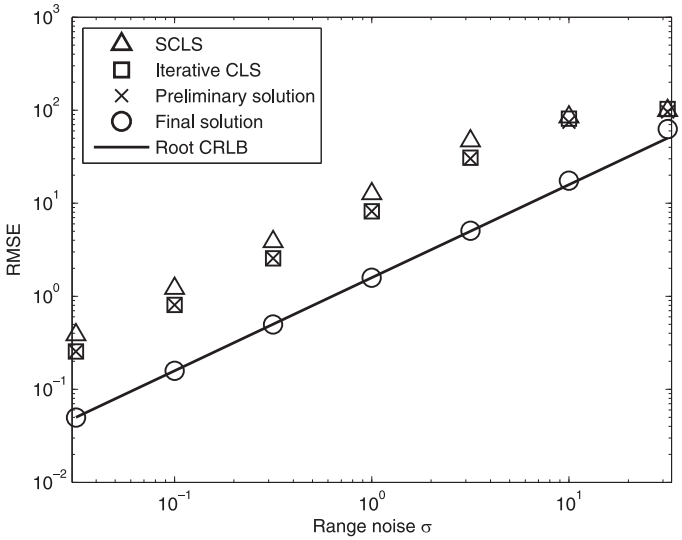

Fig. 7. Performance for orientation θ (deg) estimation in the 2D case, averaged over 200 realizations of anchor positions.

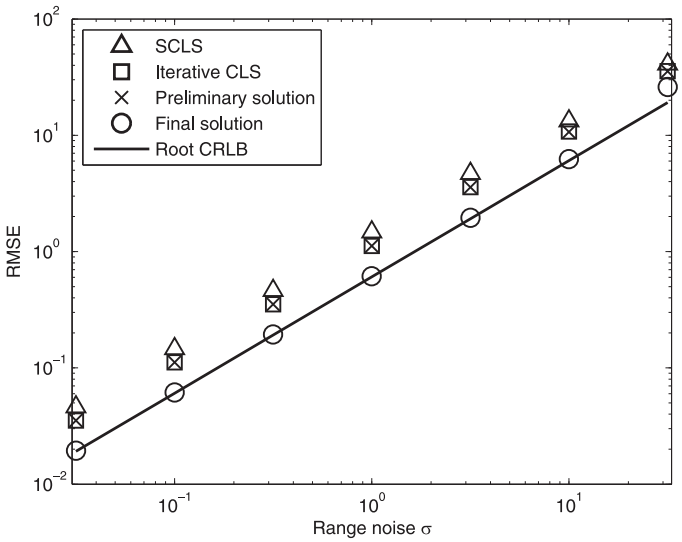

Fig. 8. Performance for position $\mathbf{t}$ estimation in the 2D case, averaged over 200 realizations of anchor positions.

it approaches the CRLB performance until the noise deviation σ is larger than 10.

The estimation bias results are shown in Figs. 9–10. It appears the method with less RMSE also has less bias. The proposed step-2 solution outperforms the others.

Fig. 11 illustrates the computation times for the estimation methods. The step-1 preliminary solution has similar computation time as SCLS. Unlike the method in Section III, the step-2 final solution only takes slightly larger complexity. The complexity of the proposed solutions is relatively stable irrespective of the noise deviations. This is not the case for the iterative CLS method due to its iterative nature. The complexity of CLS is about twice the amount of the proposed solutions and this ratio rises to more than 5 times at noise deviation $\sigma = 10$.

B. Moving Rigid Body

We use the same geometry settings as in the 3D stationary rigid body localization. The angular velocity is

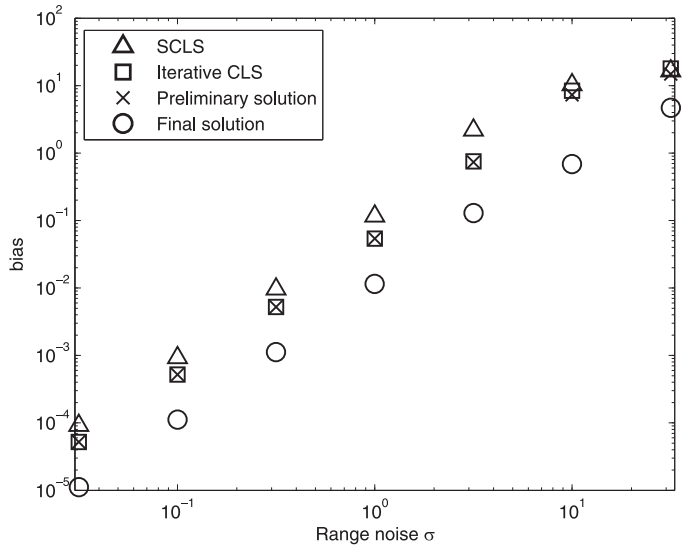

Fig. 9. Bias for orientation θ (deg) estimation in the 2D case, averaged over 200 realizations of anchor positions.

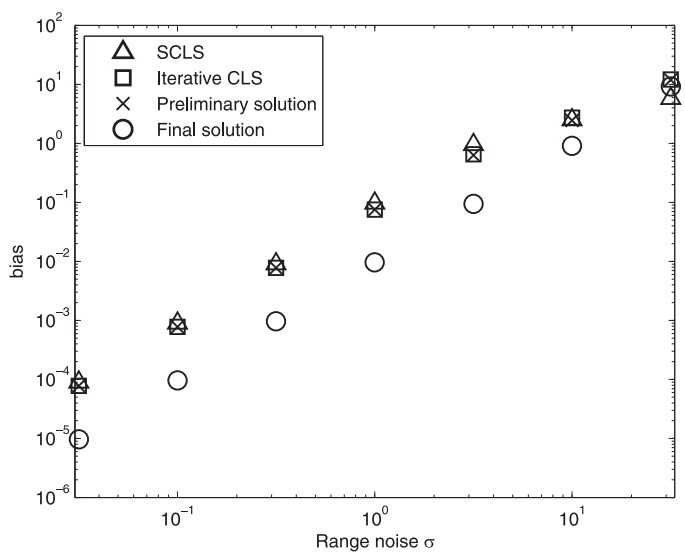

Fig. 10. Bias for position $\mathbf{t}$ estimation in the 2D case, averaged over 200 realizations of anchor positions.

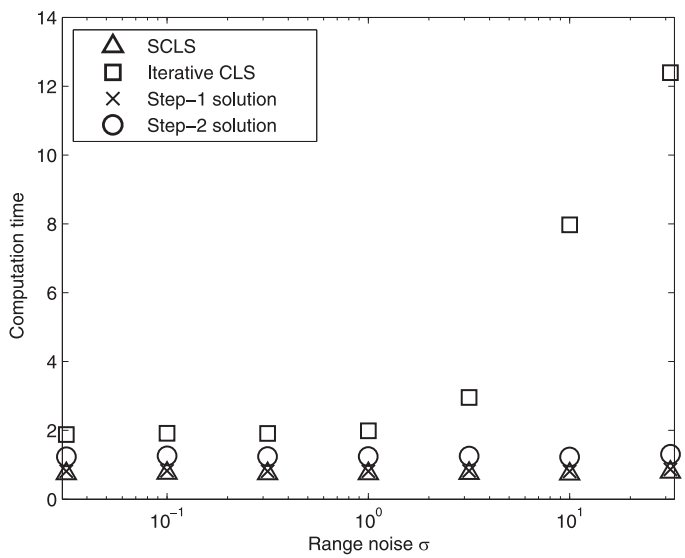

Fig. 11. Computation time (millisecond) in each Monte-Carlo run in the 2D case, averaged over 200 realizations of anchor positions.

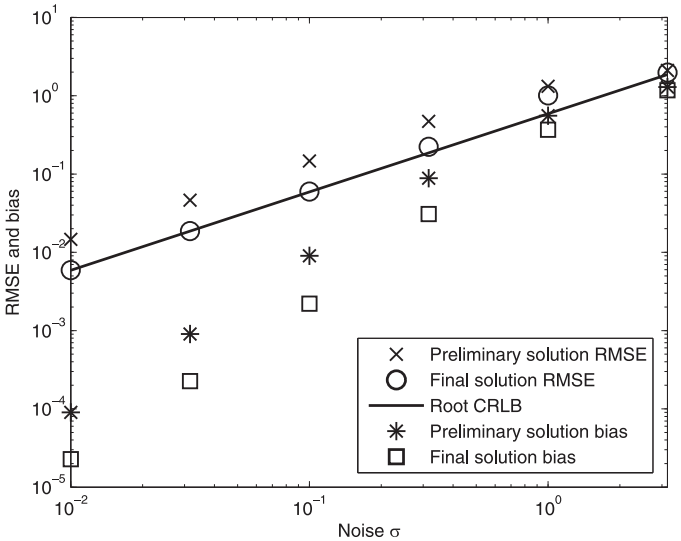

Fig. 12. RMSE and bias performance of the rotation matrix $\mathbf{Q}$ estimation for a moving rigid body in the 3D case, averaged over 200 realizations of anchor positions.

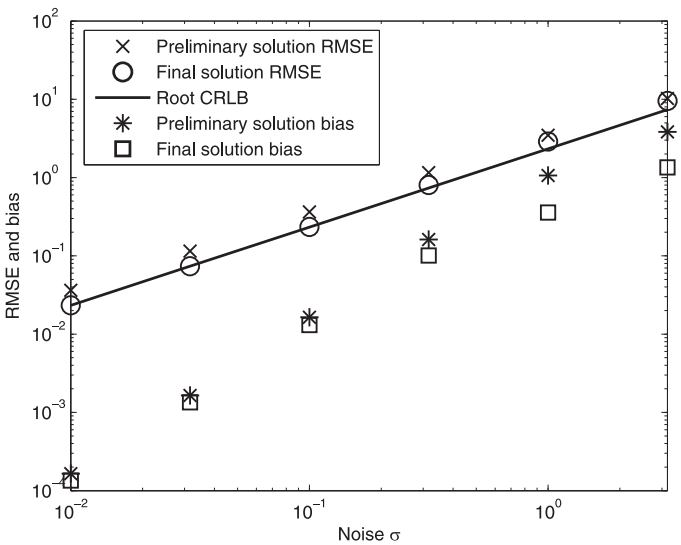

Fig. 13. RMSE and bias performance of the position $\mathbf{t}$ estimation for a moving rigid body in the 3D case, averaged over 200 realizations of anchor positions.

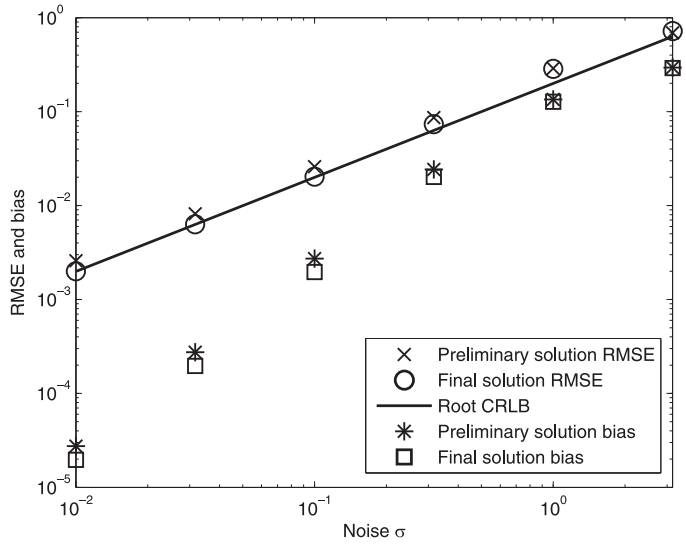

Fig. 14. RMSE and bias performance of angular velocity $\boldsymbol{\omega}$ estimation for a moving rigid body in the 3D case, averaged over 200 realizations of anchor positions.

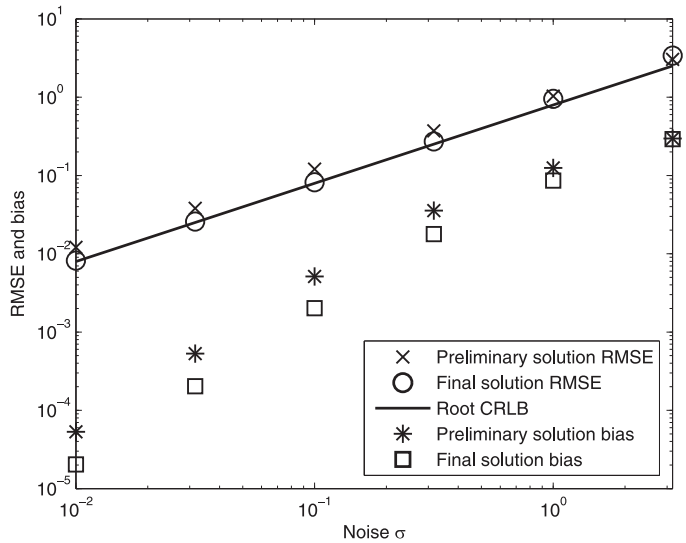

Fig. 15. RMSE and bias performance of translational velocity $\dot{\mathbf{t}}$ estimation for a moving rigid body in the 3D case, averaged over 200 realizations of anchor positions.

$\boldsymbol{\omega} = [0.1, 0.2, 0.3]^T$ rad/s and translational velocity is $\dot{\mathbf{t}} = [1, 1, 1]^T$. The Doppler measurement noise is uncorrelated with the distance measurement noise and its covariance is $\mathbf{R}_{\dot{\mathbf{v}}} = 0.1\mathbf{R}_{\mathbf{v}} = 0.1\sigma^2\mathbf{I}$.

The results are generated using the algorithm given in Section V. The initial solution $(\hat{\mathbf{Q}}, \hat{\mathbf{t}})$ needed in step-1 is obtained using both the distance and Doppler measurements. In particular, we apply the method in Appendix D to obtain the sensor position estimates and then (8) and (10) to form $(\hat{\mathbf{Q}}, \hat{\mathbf{t}})$.

Figs. 12–15 illustrate the estimation performance of RMSE and bias for $\mathbf{Q}$, $\mathbf{t}$, $\boldsymbol{\omega}$ and $\dot{\mathbf{t}}$. The step-1 solutions are far from the CRLBs, especially for $\mathbf{Q}$. The proposed step-2 solutions are able to reach the optimum performance before the noise deviation σ is larger than 0.1. The bias is relatively small compared to RMSE when the noise level is small.

For the 2D case, the step-2 refinement solution also provides performance close to the CRLB over the small noise region.

VIII. Conclusion

This paper develops methods to locate a rigid body using a number of on-the-body sensors through the distance measurements with respect to a number of anchors if it is stationary, and the Doppler as well if it is moving. The proposed method consists of an initial step and a refinement step. The initial step provides a suboptimum preliminary solution using the DAC approach and the refinement step estimates the corrections to the preliminary solution using the Euler angles formulation to achieve better estimation accuracy. Both steps involve only closed-form solution evaluations and are not iterative. We have also shown that the problem can be solved using 2 GTRS optimizations for the special case of 2D localization. For the

stationary rigid body localization, we are able to advance the previous works and provide more accurate solutions with comparable complexity. For the moving rigid body localization, we have developed closed-form solutions for obtaining not only the rotation matrix and translation vector but also the angular and translational velocities. Simulations validate the good performance of the proposed methods with accuracy approaching the CRLB under Gaussian noise over the small error region.

APPENDIX A
CRLB FOR 2D STATIONARY RIGID BODY LOCALIZATION: PARAMETERIZATION OF $\mathbf{Q}$ IN TERMS OF THE ROTATION ANGLE θ

In the 2D stationary rigid body localization algorithm presented in Section IV, the unknown vector is $[\theta, \mathbf{t}^T]^T$ since we use θ to parameterize the rotation matrix $\mathbf{Q}$. The derivatives are

$$\frac{\partial r^o_{mi}}{\partial \theta} = \frac{1}{r^o_{mi}}(\mathbf{a}_m - \mathbf{t})^T \begin{bmatrix} \sin\theta & \cos\theta \\ -\cos\theta & \sin\theta \end{bmatrix} \mathbf{c}_i \tag{50}$$

and

$$\frac{\partial r^o_{mi}}{\partial \mathbf{t}} = \frac{\mathbf{Q}\mathbf{c}_i + \mathbf{t} - \mathbf{a}_m}{r^o_{mi}}. \tag{51}$$

Stacking the rows $\frac{\partial r^o_{mi}}{\partial [\theta, \mathbf{t}^T]}$ from different measurements gives the matrix $\mathbf{J}$. The Fisher information matrix (FIM) is

$$\mathbf{FIM} = \mathbf{J}^T \mathbf{R}_{\mathbf{v}}^{-1} \mathbf{J} \tag{52}$$

whose inverse is the CRLB [34], where $\mathbf{R}_{\mathbf{v}}$ is the covariance matrix of the distance measurement noise.

APPENDIX B
CRLB FOR MOVING RIGID BODY LOCALIZATION

2D Case: The unknown parameter vector is $[\theta, \mathbf{t}^T, \omega, \dot{\mathbf{t}}^T]^T$. Since the distance equation does not contain ω and $\dot{\mathbf{t}}$, we have

$$\frac{\partial r^o_{mi}}{\partial \omega} = 0, \quad \frac{\partial r^o_{mi}}{\partial \dot{\mathbf{t}}} = \mathbf{0}.$$

Using the derivatives $\frac{\partial r^o_{mi}}{\partial \theta}$ and $\frac{\partial r^o_{mi}}{\partial \mathbf{t}}$ derived in Appendix A, we can stack the rows $\frac{\partial r^o_{mi}}{\partial [\theta, \mathbf{t}^T, \omega, \dot{\mathbf{t}}^T]}$ to form the gradient matrix $\mathbf{J}_{\mathbf{r}^o}$ for the distance measurements.

For the Doppler measurements, we have from (5),

$$\begin{aligned}
\frac{\partial \dot{r}^o_{mi}}{\partial \theta} &= -\frac{1}{r^o_{mi}}(\mathbf{t}^T[\omega]^\times - \mathbf{a}_m^T[\omega]^\times + \dot{\mathbf{t}}^T) \begin{bmatrix} \sin\theta & \cos\theta \\ -\cos\theta & \sin\theta \end{bmatrix} \mathbf{c}_i \\
&\quad - \frac{\dot{r}^o_{mi}}{r^o_{mi}} \frac{\partial r^o_{mi}}{\partial \theta}, \\
\frac{\partial \dot{r}^o_{mi}}{\partial \mathbf{t}} &= \frac{1}{r^o_{mi}}([\omega]^\times \mathbf{Q}\mathbf{c}_i + \dot{\mathbf{t}}) - \frac{\dot{r}^o_{mi}}{r^o_{mi}} \frac{\partial r^o_{mi}}{\partial \mathbf{t}}, \\
\frac{\partial \dot{r}^o_{mi}}{\partial \omega} &= \frac{1}{r^o_{mi}} \mathbf{\Phi}^T[(\mathbf{Q}\mathbf{c}_i) \otimes (\mathbf{t} - \mathbf{a}_m)], \\
\frac{\partial \dot{r}^o_{mi}}{\partial \dot{\mathbf{t}}} &= \frac{1}{r^o_{mi}}(\mathbf{Q}\mathbf{c}_i + \mathbf{t} - \mathbf{a}_m),
\end{aligned} \tag{53}$$

where $\frac{\partial r^o_{mi}}{\partial \theta}$ and $\frac{\partial r^o_{mi}}{\partial \mathbf{t}}$ are given in Appendix A and $\mathbf{\Phi}$ is defined in (39). Stacking the derivatives $\frac{\partial \dot{r}^o_{mi}}{\partial [\theta, \mathbf{t}^T, \omega, \dot{\mathbf{t}}^T]}$ forms the gradient matrix $\mathbf{J}_{\dot{\mathbf{r}}^o}$. The resulting FIM is

$$\mathbf{FIM} = \begin{bmatrix} \mathbf{J}_{\mathbf{r}^o} \\ \mathbf{J}_{\dot{\mathbf{r}}^o} \end{bmatrix}^T \mathbf{R}^{-1} \begin{bmatrix} \mathbf{J}_{\mathbf{r}^o} \\ \mathbf{J}_{\dot{\mathbf{r}}^o} \end{bmatrix}, \tag{54}$$

whose inverse is the CRLB.

3D Case: We shall first evaluate the FIM of the unknown parameter vector $\boldsymbol{\zeta} = [\mathbf{q}^T, \mathbf{t}^T, \boldsymbol{\omega}^T, \dot{\mathbf{t}}^T]^T$ without having the $SO(3)$ constraint, where $\mathbf{q} = \mathrm{vec}(\mathbf{Q})$. The gradients $\frac{\partial \dot{r}^o_{mi}}{\partial \mathbf{t}}$, $\frac{\partial \dot{r}^o_{mi}}{\partial \boldsymbol{\omega}}$ and $\frac{\partial \dot{r}^o_{mi}}{\partial \dot{\mathbf{t}}}$ are the same as those in the 2D case, where $\mathbf{\Phi}$ is given in (38). From (5),

$$\frac{\partial \dot{r}^o_{mi}}{\partial \mathbf{q}} = \frac{1}{r^o_{mi}}[\mathbf{c}_i \otimes ([\boldsymbol{\omega}]^\times \mathbf{a}_m - [\boldsymbol{\omega}]^\times \mathbf{t} + \dot{\mathbf{t}})] - \frac{\dot{r}^o_{mi}}{r^o_{mi}} \frac{\partial r^o_{mi}}{\partial \mathbf{q}} \tag{55}$$

where $\frac{\partial r^o_{mi}}{\partial \mathbf{q}} = \frac{1}{r^o_{mi}} \mathbf{c}_i \otimes (\mathbf{Q}\mathbf{c}_i + \mathbf{t} - \mathbf{a}_m)$. We can now form $\mathbf{J}_{\mathbf{r}^o}$ and $\mathbf{J}_{\dot{\mathbf{r}}^o}$, and obtain the FIM using (54).

The constrained CRLB by imposing $\mathbf{Q}$ to $SO(3)$ is obtained by the FIM together with the gradient matrix of the constraints with respect to $\boldsymbol{\zeta}$, the readers are referred to [6] for details (note that [6] omits the constraint $\det(\mathbf{Q}) = 1$ on the rotation matrix which could result in a bound that is higher than the actual. Imposing the constraint $\mathbf{Q}^T\mathbf{Q} = \mathbf{I}$ is not sufficient since it implies not only $\det(\mathbf{Q}) = 1$ representing rotation but also $\det(\mathbf{Q}) = -1$ representing reflection).

APPENDIX C
DEFINITION OF $\boldsymbol{\gamma}$ AND $\mathbf{L}$ FOR MULTIPLICATIVE CORRECTIVE ROTATION MATRIX

In general 3D case, $\boldsymbol{\gamma}$ is a 9×1 sparse vector with value 1 for the 1st, 5th and 9th elements and 0 otherwise, and $\mathbf{L}$ is a 9×3 sparse matrix with the (3, 2), (4, 3) and (8, 1) elements equal to 1, (2, 3), (6, 1) and (7, 2) elements equal to -1 and 0 otherwise.

We would like to point out that we cannot choose the Euler angle sequence (3, 1, 3) (rotates with respect to z, x, z axes in sequence) to represent $\mathbf{Q}_\delta$. Such a choice will cause the matrix $\mathbf{H}^T\mathbf{R}_{\mathbf{n}}^{-1}\mathbf{H}$ to be singular and cannot be inverted.

In 2D case, $\boldsymbol{\beta} = \theta$, $\boldsymbol{\gamma} = [1, 0, 0, 1]^T$ and $\mathbf{L} = [0, 1, -1, 0]^T$.

APPENDIX D
THE TWO-STAGE METHOD FOR LOCALIZATION USING TOA AND DOPPLER MEASUREMENTS

We shall obtain the position and velocity of each sensor individually. Following [26], the nonlinearly transformed measurement equations for the i-th sensor are

$$\epsilon_{t,m} = r^2_{mi} - \|\mathbf{a}_m\|^2 - (-2\mathbf{a}_m^T\mathbf{s}_i + \|\mathbf{s}_i\|^2) \approx 2r^o_{mi} v_{mi} \tag{56}$$

$$\epsilon_{f,m} = r_{mi}\dot{r}_{mi} - (\mathbf{s}_i^T\dot{\mathbf{s}}_i - \mathbf{a}_m^T\dot{\mathbf{s}}_i) \approx \dot{r}^o_{mi} v_{mi} + r^o_{mi}\dot{v}_{mi} \tag{57}$$

for $m = 1, 2, \ldots, M$. We solve for the unknowns $\boldsymbol{\theta}_1 = [\mathbf{s}_i^T, \|\mathbf{s}_i\|^2, \dot{\mathbf{s}}_i^T, \mathbf{s}_i^T\dot{\mathbf{s}}_i]^T$ from the matrix equation constructed from (56) and (57),

$$\boldsymbol{\epsilon}_1 = \begin{bmatrix} \boldsymbol{\epsilon}_t \\ \boldsymbol{\epsilon}_f \end{bmatrix} = \mathbf{h}_1 - \mathbf{G}_1\boldsymbol{\theta}_1 \tag{58}$$

where

$$\mathbf{h}_1 = \begin{bmatrix} r_{1i}^2 - \|\mathbf{a}_1\|^2 \\ \vdots \\ r_{Mi}^2 - \|\mathbf{a}_M\|^2 \\ r_{1i}\dot{r}_{1i} \\ \vdots \\ r_{Mi}\dot{r}_{Mi} \end{bmatrix}, \ \mathbf{G}_1 = \begin{bmatrix} -2\mathbf{a}_1^T & 1 & \mathbf{0}^T & 0 \\ \vdots & & & \\ -2\mathbf{a}_M^T & 1 & \mathbf{0}^T & 0 \\ \mathbf{0}^T & 0 & -\mathbf{a}_1^T & 1 \\ & & \vdots & \\ \mathbf{0}^T & 0 & -\mathbf{a}_M^T & 1 \end{bmatrix}. \tag{59}$$

In $\mathbf{G}_1$, $\mathbf{0}$ is a 3×1 vector of zeros. The solution is

$$\hat{\boldsymbol{\theta}}_1 = (\mathbf{G}_1^T \mathbf{W}_1 \mathbf{G}_1)^{-1} \mathbf{G}_1^T \mathbf{W}_1 \mathbf{h}_1 \tag{60}$$

where $\mathbf{W}_1 = (E[\boldsymbol{\epsilon}_1 \boldsymbol{\epsilon}_1^T])^{-1}$. $E[\boldsymbol{\epsilon}_1 \boldsymbol{\epsilon}_1^T]$ are defined by the correlations $E[\epsilon_{t,k}\epsilon_{t,l}] = 4 r_{ki}^o r_{li}^o E[v_{ki} v_{li}]$,

$$E[\epsilon_{f,k}\epsilon_{f,l}] = \dot{r}_{ki}^o \dot{r}_{li}^o E[v_{ki} v_{li}] + r_{ki}^o r_{li}^o E[\dot{v}_{ki} \dot{v}_{li}] + \dot{r}_{ki}^o r_{li}^o E[v_{ki} \dot{v}_{li}] + r_{ki}^o \dot{r}_{li}^o E[\dot{v}_{ki} v_{li}]$$

and $E[\epsilon_{t,k}\epsilon_{f,l}] = 2 r_{ki}^o \dot{r}_{li}^o E[v_{ki} v_{li}] + 2 r_{ki}^o r_{li}^o E[v_{ki} \dot{v}_{li}]$, where the noise correlation values can be obtained from the elements of $\mathbf{R}$.

From the elements of $\hat{\boldsymbol{\theta}}_1$ and their ideal relations, we can construct the matrix equation

$$\boldsymbol{\epsilon}_2 = \mathbf{h}_2 - \mathbf{G}_2 \boldsymbol{\theta}_2 \tag{61}$$

where

$$\mathbf{h}_2 = \begin{bmatrix} \hat{\boldsymbol{\theta}}_1(1:3) \odot \hat{\boldsymbol{\theta}}_1(1:3) \\ \hat{\theta}_1(4) \\ \hat{\boldsymbol{\theta}}_1(1:3) \odot \hat{\boldsymbol{\theta}}_1(5:7) \\ \hat{\theta}_1(8) \end{bmatrix}, \ \mathbf{G}_2 = \begin{bmatrix} \mathbf{I} & \mathbf{O} \\ \mathbf{1}^T & \mathbf{0}^T \\ \mathbf{O} & \mathbf{I} \\ \mathbf{0}^T & \mathbf{1}^T \end{bmatrix},$$
$$\boldsymbol{\theta}_2 = \begin{bmatrix} \mathbf{s}_i \odot \mathbf{s}_i \\ \mathbf{s}_i \odot \dot{\mathbf{s}}_i \end{bmatrix} \tag{62}$$

where $\hat{\boldsymbol{\theta}}_1(k:l)$ denotes a subvector by collecting the k-th to the l-th elements of $\hat{\boldsymbol{\theta}}_1$ and $\hat{\theta}_1(k)$ is its k-th element. In $\mathbf{G}_2$, $\mathbf{I}$ and $\mathbf{O}$ are size 3 identity and zero matrices, and $\mathbf{1}$ and $\mathbf{0}$ are length 3 vectors of unity and zero. The solution of $\boldsymbol{\theta}_2$ is

$$\hat{\boldsymbol{\theta}}_2 = (\mathbf{G}_2^T \mathbf{W}_2 \mathbf{G}_2)^{-1} \mathbf{G}_2^T \mathbf{W}_2 \mathbf{h}_2 \tag{63}$$

where

$$\mathbf{W}_2 = [\mathbf{X}(\mathbf{G}_1^T \mathbf{W}_1 \mathbf{G}_1)^{-1} \mathbf{X}^T]^{-1}. \tag{64}$$

$\mathbf{X}$ is defined by the 2×2 block form with the blocks $\mathbf{X}_{11} = \mathrm{diag}([2\mathbf{s}_i^T, 1]^T)$, $\mathbf{X}_{12} = \mathbf{O}$, $\mathbf{X}_{21} = \mathrm{diag}([\dot{\mathbf{s}}_i^T, 0]^T)$, and $\mathbf{X}_{22} = \mathrm{diag}([\mathbf{s}_i^T, 1]^T)$.

The position and velocity estimates of i-th sensor are

$$\hat{\mathbf{s}}_i = \mathrm{diag}(\mathrm{sgn}(\hat{\boldsymbol{\theta}}_1(1:3))) \left[\sqrt{\hat{\theta}_2(1)}, \sqrt{\hat{\theta}_2(2)}, \sqrt{\hat{\theta}_2(3)} \right]^T$$
$$\hat{\dot{\mathbf{s}}}_i = \hat{\boldsymbol{\theta}}_2(4:6) ./ \hat{\mathbf{s}}_i. \tag{65}$$

where $\mathrm{sgn}(*)$ is signum function and $./$ is element-wise division.

APPENDIX E
IMPLEMENTATION DETAILS FOR SCLS AND CLS

For the implementation of SCLS, we use the solution from (25) instead of (24) from [6]. The anchor positions are randomly assigned in our simulation. As a result, degenerate anchor topology may occur which leads to worse result using (24).We impose $\det(\mathbf{Q}) = 1$ when adopting orthogonal Procrustes problem technique.

For the implementation of CLS, we initialize it with the proposed step-1 solution instead of SCLS since the former gives better accuracy. The iteration of CLS stops when the relative gradient magnitude is less than 10^{-10} [37] or when the maximum number of iterations, set to 50, is reached.

ACKNOWLEDGMENT

The authors are very grateful to the associate editor and the anonymous reviewers for providing valuable comments and suggestions to improve the manuscript.

REFERENCES

[1] B. Barshan and H. F. Durrant-Whyte, "Inertial navigation systems for mobile robots," *IEEE Trans. Robot. Autom.*, vol. 11, no. 3, pp. 328–342, Jun. 1995.
[2] J. L. Crassidis, R. Alonso, and J. L. Junkins, "Optimal attitude and position determination from line-of-sight measurements," *J. Astronautic. Sci.*, vol. 48, no. 2, pp. 391–408, 2000.
[3] A. I. Mourikis, N. Trawny, S. I. Roumeliotis, A. E. Johnson, A. Ansar, and L. Matthies, "Vision-aided inertial navigation for spacecraft entry, descent, and landing," *IEEE Trans. Robot. Autom.*, vol. 25, no. 2, pp. 264–280, Apr. 2009.
[4] Y. Shen and M. Z. Win, "On the accuracy of localization systems using wideband antenna arrays," *IEEE Trans. Commun.*, vol. 58, no. 1, pp. 270–280, Jan. 2010.
[5] F. Aghili and A. Salerno, "Driftless 3-D attitude determination and positioning of mobile robots by integration of IMU with two RTK GPSs," *IEEE/ASME Trans. Mechatronics*, vol. 18, no. 1, pp. 21–31, Feb. 2013.
[6] S. P. Chepuri, G. Leus, and A.-J. van der Veen, "Rigid body localization using sensor networks," *IEEE Trans. Signal Process.*, vol. 62, no. 18, pp. 4911–4924, Sep. 2014.
[7] A. Alcocer, P. Oliveira, A. Pascoal, and J. Xavier, "Estimation of attitude and position from range-only measurements using geometric descent optimization on the special Euclidean group," in *Proc. 9th Int. Conf. Inf. Fusion*, Jul. 2006, pp. 1–8.
[8] A. Alcocer, P. Oliveira, A. Pascoal, R. Cunha, and C. Silvestre, "A dynamic estimator on $SE(3)$ using range-only measurements," in *Proc. 47th IEEE Conf. Dec. Control*, Dec. 2008, pp. 2302–2307.
[9] K. Pahlavan, X. Li, and J.-P. Makela, "Indoor geolocation science and technology," *IEEE Commun. Mag.*, vol. 40, no. 2, pp. 112–118, Feb. 2002.
[10] P. Biswas, T.-C. Liang, K.-C. Toh, Y. Ye, and T.-C. Wang, "Semidefinite programming approaches for sensor network localization with noisy distance measurements," *IEEE Trans. Autom. Sci. Eng.*, vol. 3, no. 4, pp. 360–371, Oct. 2006.
[11] Y. Shen and M. Z. Win, "Fundamental limits of wideband localization-Part I: A general framework," *IEEE Trans. Inf. Theory*, vol. 56, no. 10, pp. 4956–4980, Oct. 2010.
[12] Y. Shen and M. Z. Win, "Fundamental limits of wideband localization–Part II: Cooperative framework," *IEEE Trans. Inf. Theory*, vol. 56, no. 10, pp. 4981–5000, Oct. 2010.
[13] M. Z. Win, A. Conti, S. Mazuelas, Y. Shen, W. M. Gifford, D. Dardari, and M. Chiani, "Network localization and navigation via cooperation," *IEEE Commun. Mag.*, vol. 49, no. 5, pp. 56–62, May 2011.
[14] Y. Shen, S. Mazuelas, and M. Z. Win, "Network navigation: Theory and interpretation," *IEEE J. Sel. Areas Commun.*, vol. 30, no. 9, pp. 1823–1834, Oct. 2012.
[15] J. Diebel, "Representing attitude: Euler angles, unit quaternions, and rotation vectors," *Matrix*, vol. 58, pp. 15–16, 2006.
[16] E. Foxlin, "Pedestrian tracking with shoe-mounted inertial sensors," *IEEE Comput. Graph. Appl. Mag.*, vol. 25, no. 6, pp. 38–46, Nov.-Dec. 2005.

[17] S. Mazuelas, Y. Shen, and M. Z. Win, "Belief condensation filtering," *IEEE Trans. Signal Process.*, vol. 61, no. 18, pp. 4403–4415, Sep. 2013.
[18] K. Plarre1 and P. R. Kumar, "Tracking objects with networked scattered directional sensors," *EURASIP J. Adv. Signal Process.*, vol. 2008, pp. 1–10, 2008.
[19] S. P. Chepuri, A. Simonetto, G. Leus, and A. J. Van der Veen, "Tracking position and orientation of a mobile rigid body," in *Proc. IEEE 5th Int. Workshop Computat. Adv. Multi-Sensor Adapt. Process. (CAMSAP)*, Dec. 2013, pp. 37–40.
[20] J. S. Abel, "A divide and conquer approach to least-squares estimation," *IEEE Trans. Aerosp. Electron. Syst.*, vol. 26, no. 2, pp. 423–427, Mar. 1990.
[21] W. Gander, "Least squares with a quadratic constraint," *Numer. Math.*, vol. 36, no. 3, pp. 291–307, 1980.
[22] G. Golub and U. Matt, "Quadratically constrained least squares and quadratic problems," *Numer. Math.*, vol. 59, no. 1, pp. 561–580, 1991.
[23] J. J. Moré, "Generalizations of the trust region problem," *Optim. Methods Softw.*, vol. 2, pp. 189–209, 1993.
[24] A. Beck, P. Stoica, and J. Li, "Exact and approximate solutions for source localization problems," *IEEE Trans. Signal Process.*, vol. 56, no. 5, pp. 1770–1778, May 2008.
[25] R. A. Horn and C. R. Johnson, *Topics in Matrix Analysis*. Cambridge, U.K.: Cambridge University Press, 1991.
[26] K. C. Ho and W. Xu, "An accurate algebraic solution for moving source location using TDOA and FDOA measurements," *IEEE Trans. Signal Process.*, vol. 52, no. 9, pp. 2453–2463, Sep. 2004.
[27] Y. T. Chan and K. C. Ho, "A simple and efficient estimator for hyperbolic location," *IEEE Trans. Signal Process.*, vol. 42, no. 8, pp. 1905–1915, Aug. 1994.
[28] Z. Ma and K. C. Ho, "TOA localization in the presence of random sensor position errors," in *Proc. Acoust., Speech, Signal Process. (ICASSP)*, Prague, Czech Republic, May 2011, pp. 2468–2471.
[29] S. Chen and K. C. Ho, "Reaching asymptotic efficient performance for squared processing of range and range difference localizations in the presence of sensor position errors," in *Proc. IEEE Int. Conf. Acoust., Speech, Signal Process.*, Florence, Italy, May 2014, pp. 1419–1423.
[30] S. Umeyama, "Least-squares estimation of transformation parameters between two point patterns," *IEEE Trans. Pattern Anal. Mach. Intell.*, vol. 13, no. 4, pp. 376–380, Apr. 1991.
[31] D. W. Eggert, A. Lorusso, and R. B. Fisher, "Estimating 3-D rigid body transformations: A comparison of four major algorithms," *Mach. Vis. Appl.*, vol. 9, no. 5–6, pp. 272–290, Mar. 1997.
[32] S. Chen and K. C. Ho, "Achieving asymptotic efficient performance for squared range and squared range difference localizations," *IEEE Trans. Signal Process.*, vol. 61, no. 11, pp. 2836–2849, Jun. 2013.
[33] H. L. Van Trees, *Detection, Estimation, and Modulation Theory, Part I*. New York, NY, USA: Wiley, 1968.
[34] S. M. Kay, *Fundamentals of Statistical Signal Processing: Estimation Theory*. Englewood Cliffs, NJ, USA: Prentice-Hall, 1993.
[35] K. W. Cheung, H. C. So, W. K. Ma, and Y. T. Chan, "Least squares algorithms for time-of-arrival-based mobile location," *IEEE Trans. Signal Process.*, vol. 52, no. 4, pp. 1121–1228, Apr. 2004.
[36] H.-W. Wei, Q. Wan, Z.-X. Chen, and S.-F. Ye, "A novel weighted multidimensional scaling analysis for time-of-arrival-based mobile location," *IEEE Trans. Signal Process.*, vol. 56, no. 7, pp. 3018–3022, Jul. 2008.
[37] T. Viklands, "Algorithms for the weighted orthogonal Procrustes problem and other least squares problems," Ph.D. dissertation, Umea Univ., Umea, Sweden, 2008.

Shanjie Chen (S'11) received the B.S. degree in electrical engineering from the Nanjing Agricultural University, Nanjing, China, in 2007, and M.S. degree in electrical engineering from the University of Science and Technology of China, Hefei, China, in 2010. He is currently working towards the Ph.D. degree with the Department of Electrical and Computer Engineering, University of Missouri, Columbia, USA.

His current research interests include localization, tracking, and navigation.

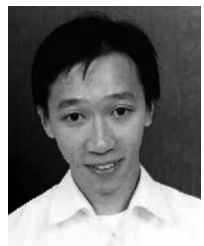

K. C. Ho (M'91–SM'00–F'09) was born in Hong Kong. He received the B.Sc. degree with First Class Honors in Electronics and the Ph.D. degree in Electronic Engineering in 1988 and 1991, respectively.

He was a research associate in the Royal Military College of Canada from 1991 to 1994. He joined the Bell-Northern Research, Montreal, QC, Canada, in 1995 as a member of scientific staff. He was a faculty in the Department of Electrical Engineering at the University of Saskatchewan, Saskatoon, Canada, from September 1996 to August 1997. Since September 1997, he has been with the University of Missouri and is currently a Professor in the Electrical and Computer Engineering Department. His research interests are in sensor array processing, source localization, subsurface object detection, wireless communications and adaptive processing. He was very active in the development of the ITU-T Standard Recommendations from 1995 to 2012. He was the Rapporteur of ITU-T Q15/SG16: Voice Gateway Signal Processing Functions and Circuit Multiplication Equipment/ Systems from 2009 to 2012, and the Associate Rapporteur of ITUT Q16/SG16: Speech Enhancement Functions in Signal Processing Network Equipment in 2012. He was the Editor of the ITU-T Recommendations G.160: Voice Enhancement Devices from 2006 to 2012, G.168: Digital Network Echo Cancellers from 2000 to 2012 and G.799.2: Mechanism for Dynamic Coordination of Signal Processing Network Equipment from 2004 to 2009.

Dr. Ho is a Technical Co-Chair of the IEEE International Conference on Acoustics, Speech and Signal Processing 2016 (ICASSP2016). Dr. Ho has served as the Chair (2013–2014) and Vice-Chair (2011–2012) of the Sensor Array and Multichannel (SAM) Technical Committee of the IEEE Signal Processing Society. He was in the organizing committees of the IEEE SAM 2008 Workshop and the IEEE CAMSAP 2011. He was an Associate Editor of the IEEE TRANSACTIONS ON SIGNAL PROCESSING (2009–2013, 2003–2006) and the IEEE SIGNAL PROCESSING LETTERS (2004–2008). He received the Senior Faculty Research Award in 2014 and 2009, the Junior Faculty Research Award in 2003 and the Teaching Award in 2006 from the College of Engineering at the University of Missouri. He is an inventor of 20 patents in the United States, Canada, Europe, and Asia on geolocation and signal processing for wireless communications.